AD-A161 455 KINETICS AND MECHANISMS OF CREEP IN SINTERED ALPHA SSILICON CARBIDE AND NI.. (U) NORTH CAROLINA STATE UNIV AT RALEIGH SCHOOL OF ENGINEERING R F DAVIS 10 SEP 85 1/1

UNCLASSIFIED ARO-18434.8-MS NSF-DMR81-20004 F/G 20/11 NL

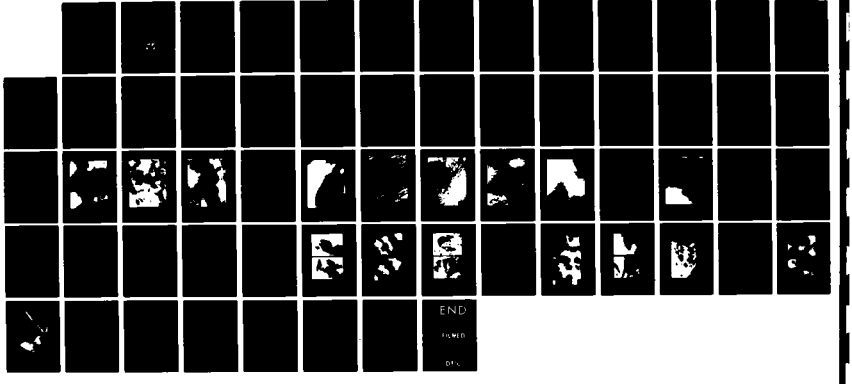

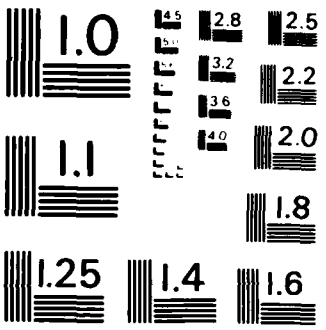

ARO 18434.8-MS

FINAL REPORT

on

KINETICS AND MECHANISMS OF CREEP IN SINTERED ALPHA SILICON CARBIDE AND NIOBIUM CARBIDE

Supported by

SF (DMR-812-0804) and ARO (MIPR's 43-48, 127-83, 141-84)

August, 1985

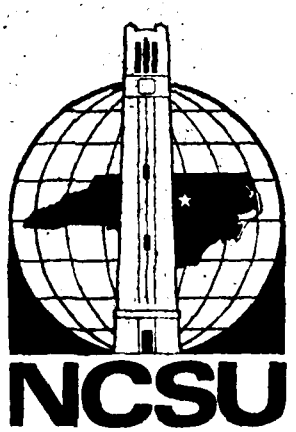

School of Engineering

North Carolina State University

Raleigh, North Carolina

FINAL REPORT

on

KINETICS AND MECHANISMS OF CREEP IN SINTERED ALPHA SILICON CARBIDE AND NIOBIUM CARBIDE

Supported by

NSF (DMR-812-0804) and ARO (MIPR's 43-48, 127-83, 141-84)

August, 1985

MASTER COPY - FOR REPRODUCTION PURPOSES

UNCLASSIFIED
SECURITY CLASSIFICATION OF THIS PAGE (When Data Entered)

REPORT DOCUMENTATION PAGE

READ INSTRUCTIONS BEFORE COMPLETING FORM

1. REPORT NUMBER: ARO 18434.8-MS	2. GOVT ACCESSION NO.: N/A
3. RECIPIENT'S CATALOG NUMBER: N/A	
4. TITLE (and Subtitle): Kinetics and Mechanisms of Creep in Sintered Alpha Silicon Carbide and Niobium Carbide	5. TYPE OF REPORT & PERIOD COVERED: Final, May 1, 1982-June 15, 1985
	6. PERFORMING ORG. REPORT NUMBER:
7. AUTHOR(s): Robert F. Davis	8. CONTRACT OR GRANT NUMBER(s): MIPR's 43-82, 127-83, 141-84
9. PERFORMING ORGANIZATION NAME AND ADDRESS: North Carolina State University, Hillsborough Street, Raleigh, NC 27695-7907	10. PROGRAM ELEMENT, PROJECT, TASK AREA & WORK UNIT NUMBERS:
11. CONTROLLING OFFICE NAME AND ADDRESS: U. S. Army Research Office, Post Office Box 12211, Research Triangle Park, NC 27709	12. REPORT DATE: September 18, 1985
	13. NUMBER OF PAGES: 56
14. MONITORING AGENCY NAME & ADDRESS (if different from Controlling Office):	15. SECURITY CLASS. (of this report): Unclassified
	15a. DECLASSIFICATION/DOWNGRADING SCHEDULE:

16. DISTRIBUTION STATEMENT (of this Report)

Approved for public release; distribution unlimited.

17. DISTRIBUTION STATEMENT (of the abstract entered in Block 20, if different from Report)

NA

18. SUPPLEMENTARY NOTES

The view, opinions, and/or findings contained in this report are those of the author(s) and should not be construed as an official Department of the Army position, policy, or decision, unless so designated by other documentation.

19. KEY WORDS (Continue on reverse side if necessary and identify by block number)

Silicon Carbide
Niobium Carbide
Creep
Hot Isostatic pressing
dislocations
climb
stacking faults
diffusion
grain boundary sliding

20. ABSTRACT (Continue on reverse side if necessary and identify by block number)

Constant stress compressive creep studies and complementary TEM research have been conducted on sintered α-SiC and on dense polycrystalline $NbC_{0.737}$ to determine the kinetics and the mechanisms of deformation as a function of temperature and stress. In the former material, the values of the stress exponents of 1.44-1.71 indicate that either viscous flow or grain boundary sliding is controlling creep. However, the values of the activation energies (≅400kJ/mol below 1920K and ≅850 kJ/mol above 1920K) coupled with the TEM studies which show the presence of considerable dislocation glide activity and the formation

DD FORM 1 JAN 73 1473 EDITION OF 1 NOV 65 IS OBSOLETE

UNCLASSIFIED
SECURITY CLASSIFICATION OF THIS PAGE (When Data Entered)

TABLE OF CONTENTS

A-1

LIST OF FIGURES

SECTION II

List of Figures (Con't)

List of Figures (Con't)

Page No.

LIST OF TABLES

SECTION II

SECTION III

I. STATEMENT OF PROBLEM

The principal objective of this research program was the determination of the kinetics and mechanisms of steady-state creep in polycrystalline sintered alpha silicon carbide and polycrystalline hot isostatically pressed niobium carbide via constant stress compressive creep experiments and extensive chemical, structural and microstructural analyses of the as-received, annealed and crept samples.

II. SILICON CARBIDE RESEARCH

A. Results and Discussion of the Steady-state Creep Experiments

1. Determination of the Stress Exponents

In order to accurately determine in sintered α-SiC the kinetics of primary and steady-state creep and to obtain an indication of the controlling mechanism as a function of temperature and stress in this latter stage of deformation, long term constant stress creep experiments have been conducted in an argon atmosphere. Figures 1, 2 and 3 show the resulting creep curves obtained for the purpose of determining the steady-state stress exponent at 1820K, 1923K and 2020K over a range of stresses. A perusal of these curves and the composite plot of Figure 4 of the results in terms of the steady-state creep rate ($\dot{\varepsilon}$) as a function of the applied stress (σ)/shear modulus (G) ratio shows that both the true strain and strain rate are very low for the sample crept at 1820K. This very low rate of strain (10^{-9} - 4×10^{-9}/sec) is near the resolution limit of the LVDT; thus, the accuracy of the curve for 1820K is slightly affected by any stray electrical signals and thermal fluctuations experienced by the LVDT. These reasons are the explanation for the roughness in the curve of Figure 1 as compared to the higher temperature curves of Figures 2 and 3.

Another noteworthy point regarding the aforenoted creep curves is that primary creep occurs at all stress levels at all temperatures. Although this stage is difficult to resolve in these curves, a comparison of each segment of each curve from enlarged plots shows that the magnitude of the primary creep is always greatest during the first segment of creep. The total strain in this stage of creep normally decreases with increasing stress (see e.g., Figure 3).

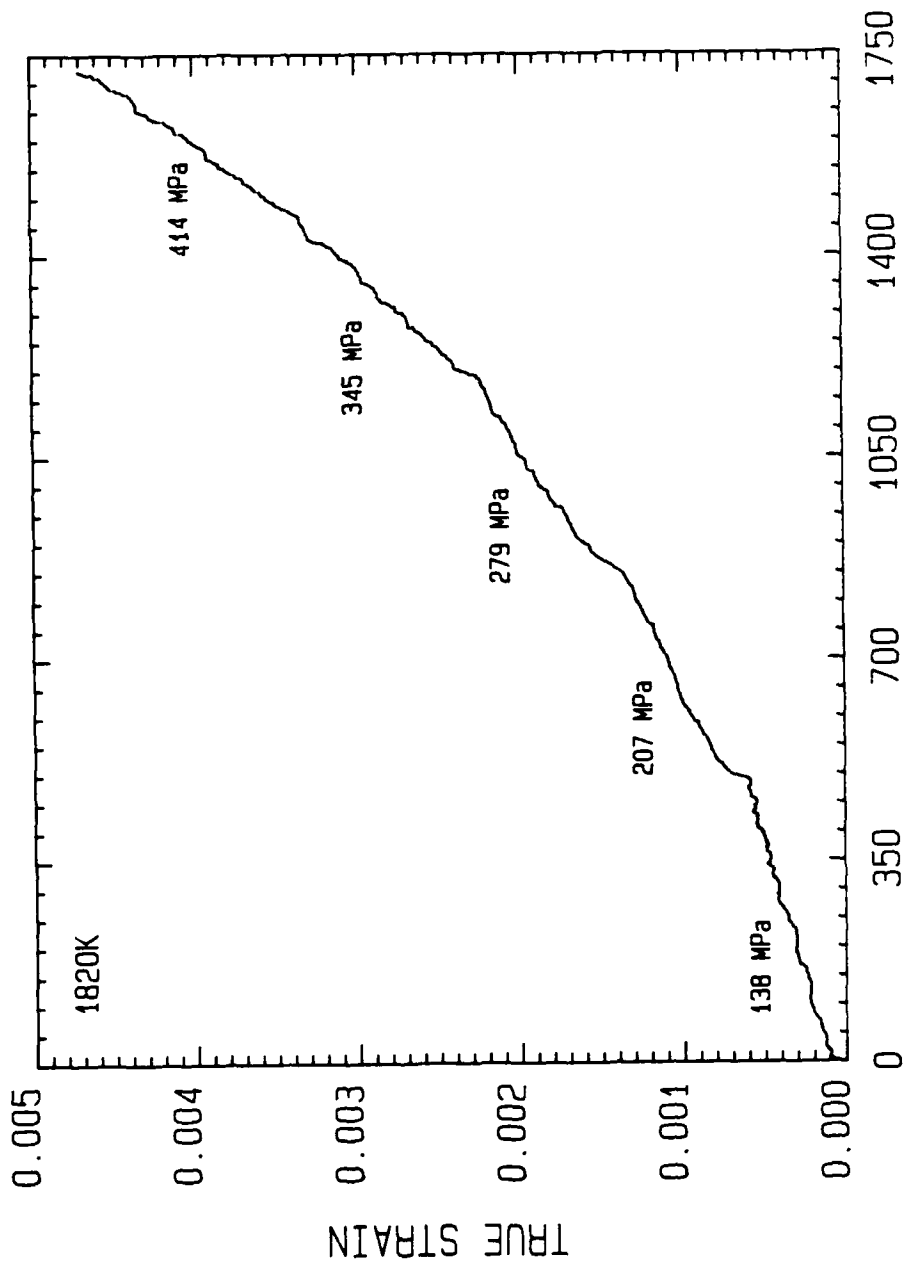

Figure 1: Creep curves sequentially obtained at 1820K and the five different stresses shown in the graph.

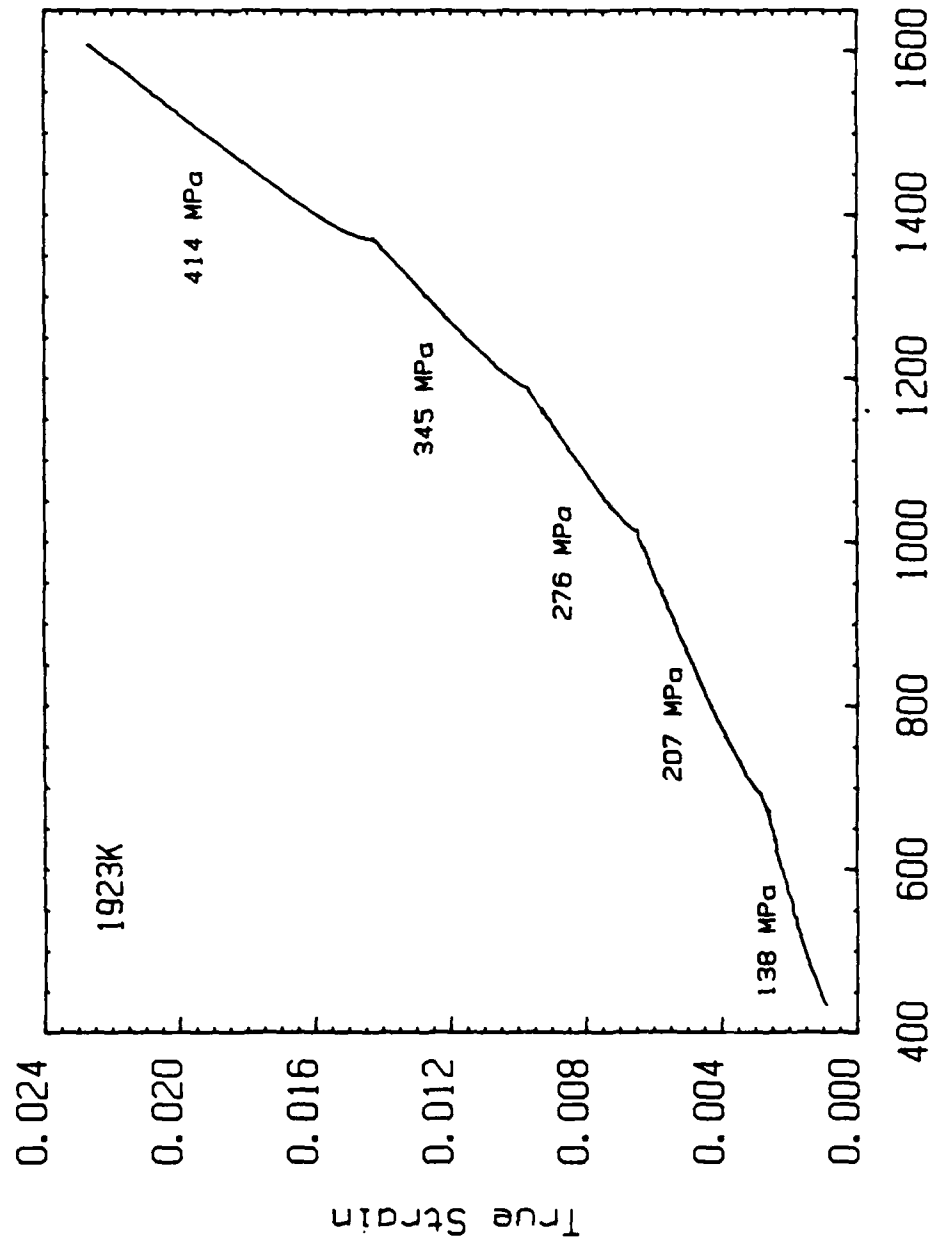

Figure 2: Creep curves sequentially obtained at 1923K and the the five different stresses shown in the graph.

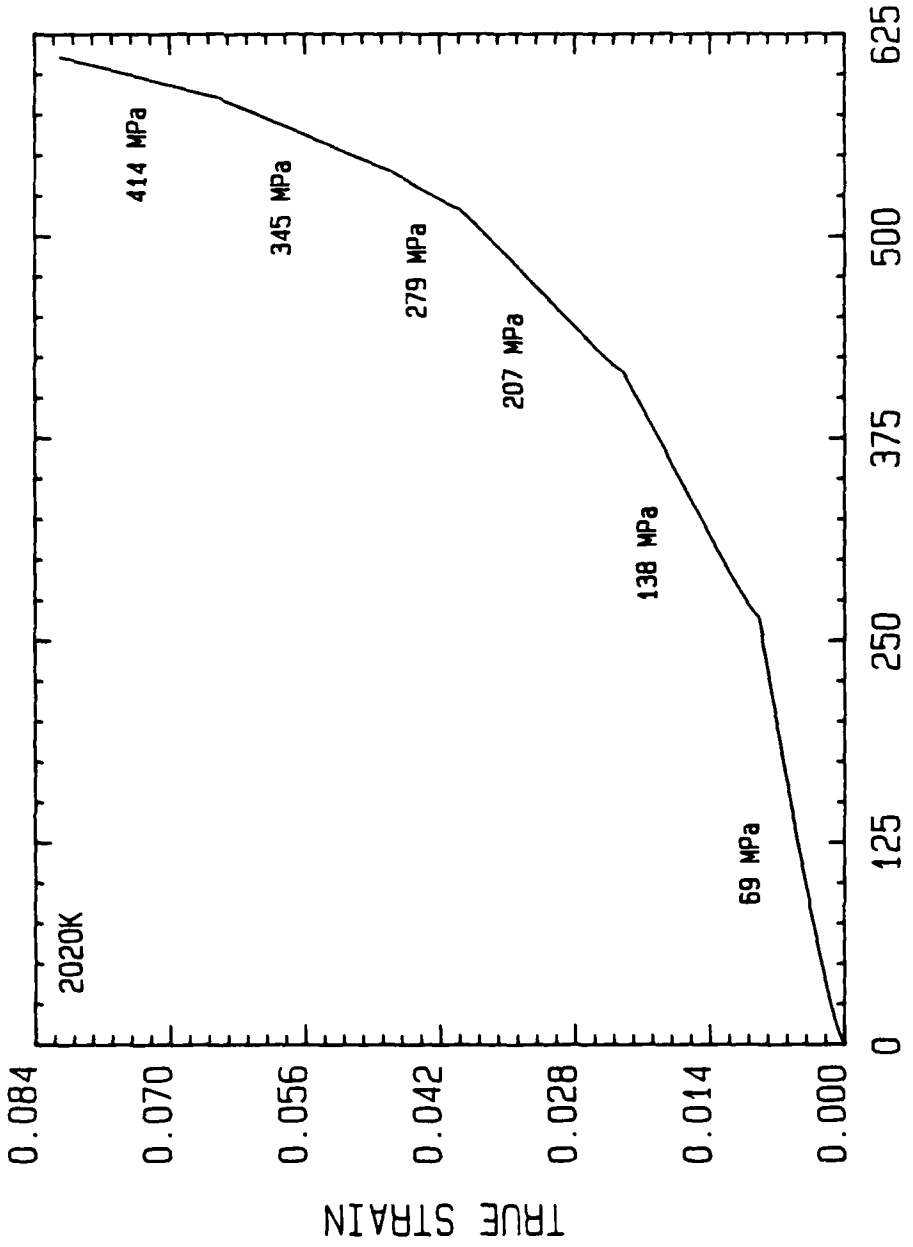

Figure 3: Creep curves sequentially obtained at 2020K and the six different stresses shown on the graph.

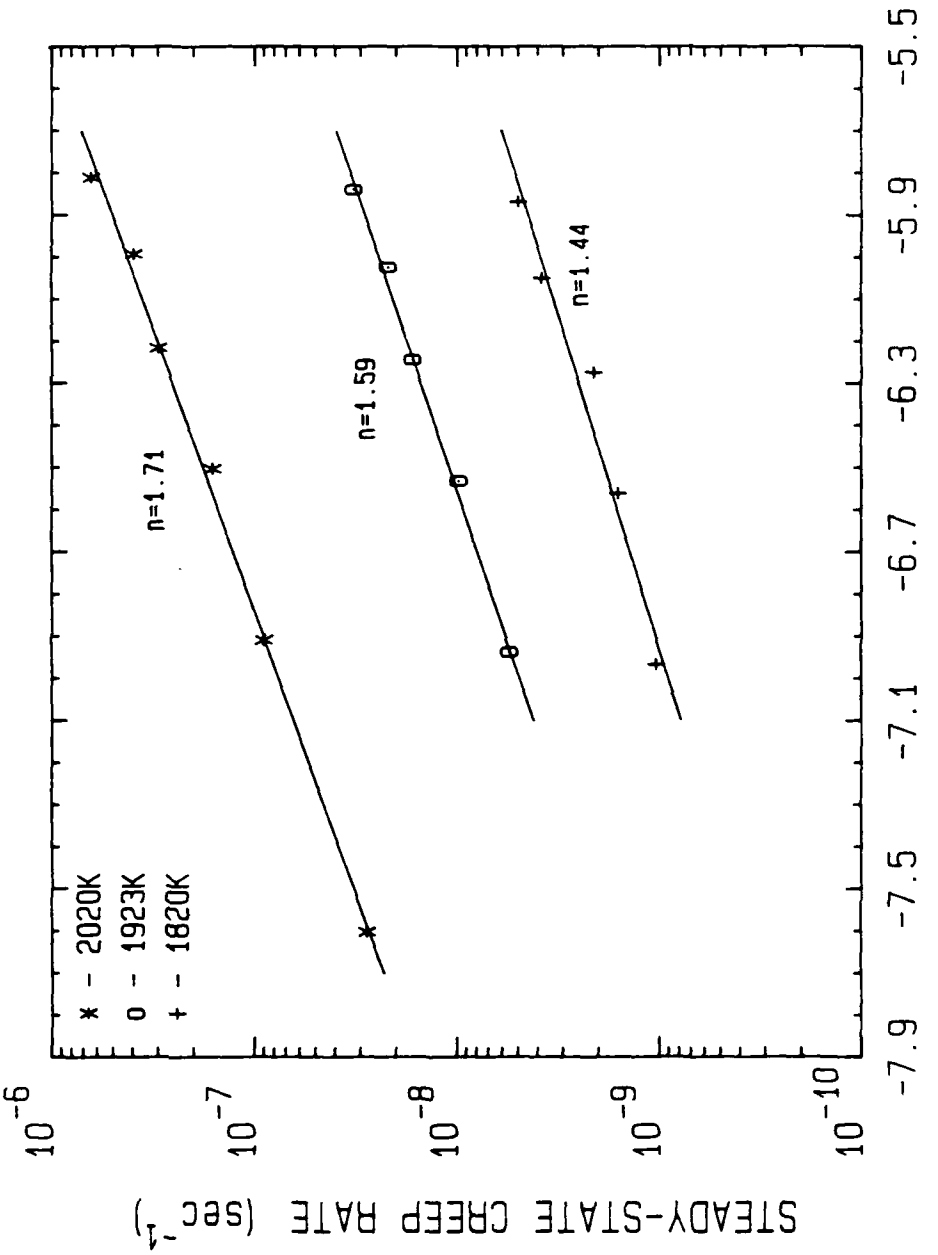

Figure 4: Steady-state creep rate values as a function of stress/G using data from the creep runs at 1820K, 1923K and 2020K.

The last segment at 1923K is an apparent anomaly, the reason for which is not known. Nevertheless, the very existence of the primary creep stage is indicative of work hardening via dislocation processes. The proof of this statement will be forthcoming in the examination of the TEM evidence.

Figure 4 also shows that the values of the stress exponent (n) are not interger numbers and increase with temperature. This information points to the existence of more than one mechanism of steady-state creep and to the gradual change in the dominant mechanism as a function of temperature. The constancy in slope at each temperature indicates that neither the dominant or the controlling mechanism is changing as a function of stress up to 414MPa. The low values of n point either to a diffusion-controlled mechanism or to the existence of viscous flow, as a result of, for example, an amorphous grain boundary phase. To date, no grain boundary phase of any type has been observed in this material via Auger or high resolution TEM techniques; thus, one must tentatively assume the measured n values point to a diffusion process as the mechanism controlling creep.

However, the assumption that a diffusion mechanism (grain boundary or lattice) is controlling steady-state creep presents other problems, in light of the present data. The current understanding of diffusion-accomodated grain boundary sliding is that dislocations in the boundaries glide and climb in response to the shear stresses in the boundaries as a result of the applied load on the sample. If the resultant sliding is to occur without the formation of corrugated grain boundaries and the formation of porosity on the boundaries and voids at the triple points, diffusion in the boundaries and/or through the lattice must occur concurrently from points on the boundary in compression to analogous areas in tension in order to cause changes in grain shape. If the

boundaries are not perfect sources and sinks for vacancies, the n value is predicted and experimentally found to be approximately 2. This is usually the case for diffusion-controlled creep at low-to-moderate temperatures. As the temperature is increased, the boundaries become more efficient generators and absorbers of vacancies and the N value normally approaches or equals 1. However, the results of Figure 4 show that the value of N in the sintered α-SiC increases slightly with temperature which is counter to that expected from the previous discussion. The precise reason(s) for this phenomenen is (are) not known; however additional discussion regarding this matter will be presented following the presentation of the data for activation energies and the TEM results.

2. Determination of the Activation Energies

Additional information regarding the controlling creep mechanisms can be obtained from the determination of the activation energy for deformation as a function of stress and comparing this data with known values of this parameter for lattice, grain boundary and, if known, pipe diffusion along dislocation cores. To this end, Figures 5-7 show the data for primary and steady-state creep as function of time for several temperatures at the constant stresses of 179, 345 and 414 MPa. As in the creep experiments to determine the stress exponents, a major portion of the primary creep occurred in the first segment, however, it decreased in amount with each increase in temperature until essentially no primary creep was observed above 2000K at any of the stresses employed. One will also note that the slopes of these curves change only slightly up to and including 1920K. However, above this approximate temperature the strain rate increases markedly with each increase in temperature. These effects of temperature on strain rate are shown for each of

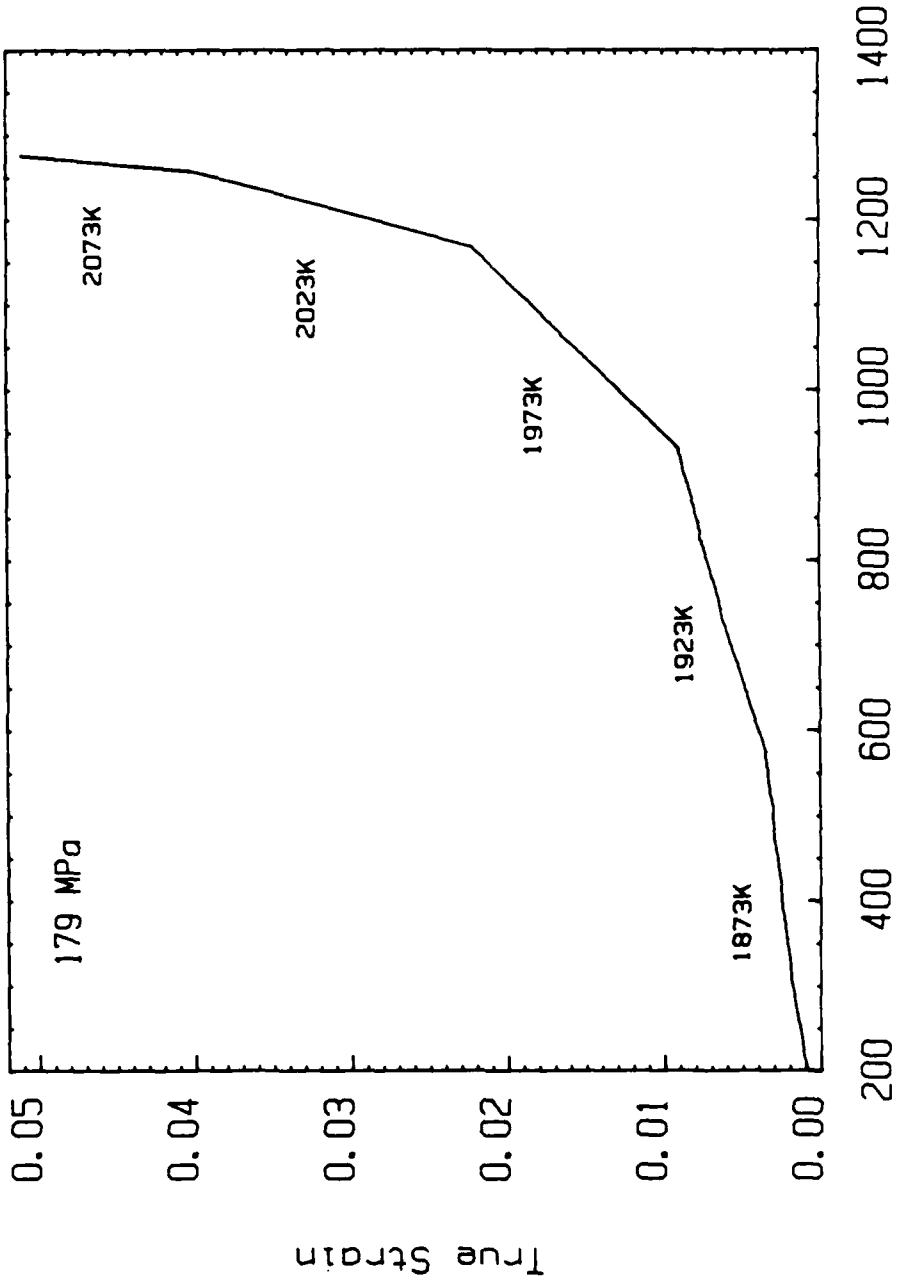

Figure 5: Creep curves sequentially obtained at 179MPa and the five different temperatures shown on the graph.

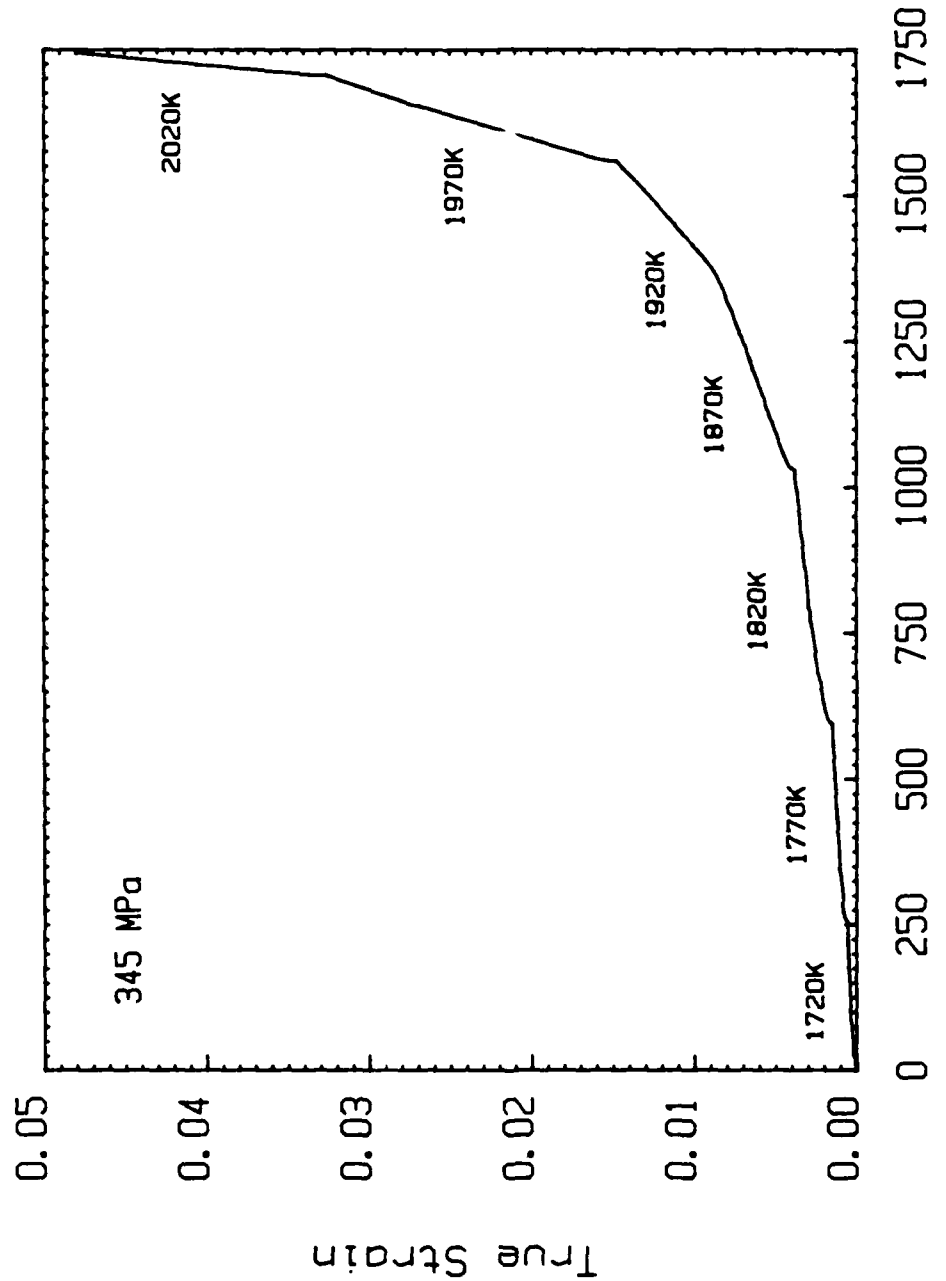

Figure 6 : Creep curves sequentially obtained at 345MPa and the seven different temperatures shown on the graph.

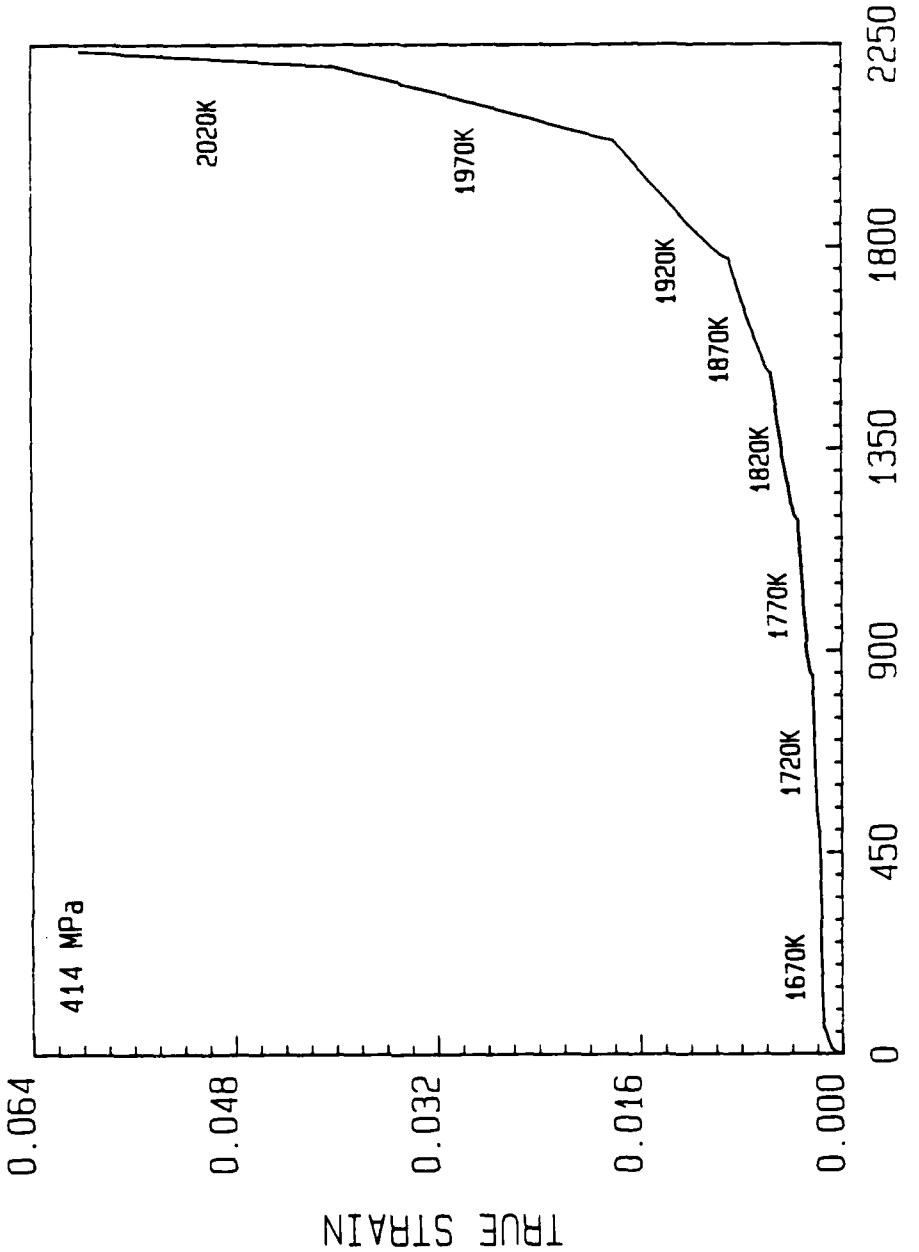

Figure 7: Creep curves sequentially obtained at 414 MPa nad the eight different temperatures shown on the graph.

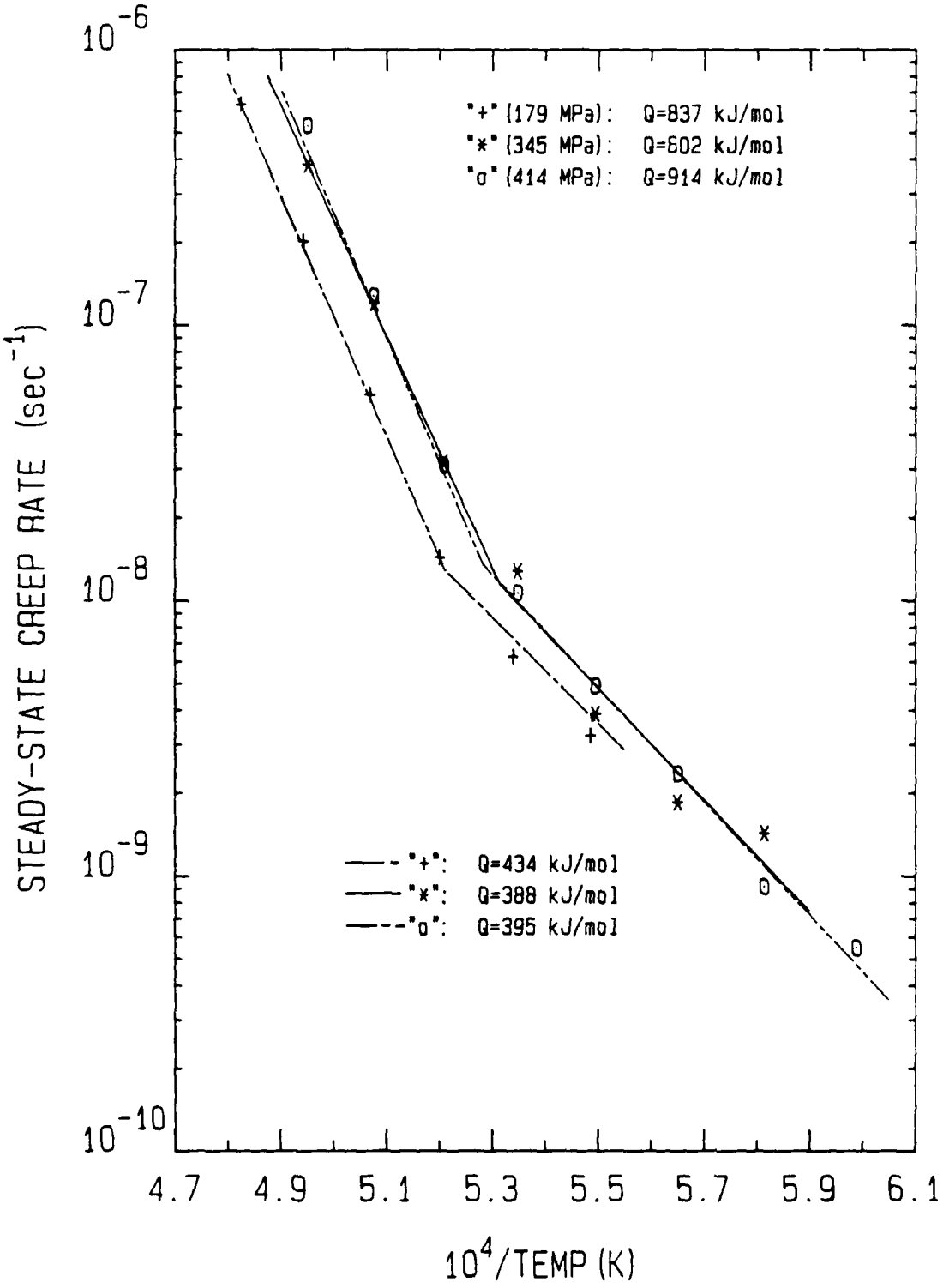

Figure 8: Steady-state creep rate values as a function of $10^4/T$ using data from the creep runs shown in Figures 5-7.

the stresses in Figure 8. Below 1920K the activation energy falls in the range of 388-434 kJ/mole; above this temperature, the values of Q are substantially higher and in the range of 837-914 kJ/mole. Furthermore, the transition temperature from one controlling mechanism to another decreases with increasing stress as shown in Figure 8.

The activation energies for self-diffusion of ^{14}C and ^{30}Si and ^{14}C boundary diffusion in SiC have been measured in this laboratory and are presented in Table I for undoped materials.

Table I. Activation energies for diffusion of ^{14}C and ^{30}Si in SiC.

DIFFUSING SPECIES	TYPE OF DIFFUSION	TYPE OF MATERIAL	Q(kJ/mole)
^{14}C	Self	Alpha Single Crystal	715±0.5
^{30}Si	Self	Alpha Single Crystal	697±15.7
^{14}C	Boundary	CVD (β) polycrystal	564

The value of activation energy for steady-state creep below ≅1920K are somewhat lower than those measured for boundary diffusion of ^{14}C. However, the latter value was measured in a highly defective polycrystalline material derived by chemical vapor deposition; whereas, the grain boundaries in the B-doped sintered α-SiC material may possess a very different character with a correspondingly lower diffusion rate. One may therefore postulate that creep is controlled by boundary diffusion below ≅1920K and at moderate stresses.

By contrast the values of Q for steady-state creep are higher than those measured for self-diffusion via lattice processes in pure α-SiC single crystals. Nevertheless from previous experience with creep in other silicon carbides the Q values for creep are believed to be much too high for all dislocation processes except climb via lattice diffusion. Thus from steady-state data alone, one would conjecture that boundary or lattice diffusion processes are controlling creep, depending on the temperature. However, if diffusion is the dominant factor in the control of creep, one should observe very little if any primary creep. Nevertheless, the presence of this stage of creep is very obvious, especially at the outset of the first segment in every creep curve. As such a study of this initial segment has been conducted at temperatures above and below the ≅1920K knee on samples annealed at the particular temperature of creep for 260kS (72 hours) and on those which had been rapidly cooled from 2373K, reheated to the temperature of creep and the load immediately applied.

B. Primary Creep Experiments

The purpose of the aforementioned study of the first stage of creep was to determine if annealing prior to loading had any effect on the creep rate

and the amount of total strain in this primary regime. It was reasoned that the high temperature (2373K) anneal used on all samples to establish the grain size would produce a larger number of vacancies which would be available for diffusion during the early part of the creep before an equilibrium vacancy concentration could be established. Thus, if lattice diffusion via a vacancy process were the controlling mechanism, the unannealed material would be expected to initially show a faster creep rate than the annealed material having a smaller number of vacancies. Furthermore, precipitation of a B-containing phase (the convergent beam electron diffraction patterns correspond to either B_4C or a B_xSi_yC solid solution) noted very early in this study to occur rather rapidly in the first primary creep stage may also be playing an important role in changing the controlling creep mechanism. If this conjecture is true, the material annealed at the temperature of creep would already contain the precipitates. Thus creep in this material would be measurably affected if the movement of dislocations were initially the dominant factor (and thus the cause of primary creep) but subsequent interaction with the precipitates pinned the dislocations and therefore caused a change from a dislocation-controlled process to one controlled by another mechanism, e.g., diffusion.

An examination of the results of four of the short term primary creep experiments (which also allowed the samples to enter the steady-state creep state in order to determine the end of the primary stage) presented in Figures 9 and 10 show that measurable differences do occur in the creep rate and total amount of strain between the samples annealed at the temperature of creep and on analogous but unannealed SiC samples at temperatures above and below the knee of the activation energy curve. (The same stress of 276MPa was used in

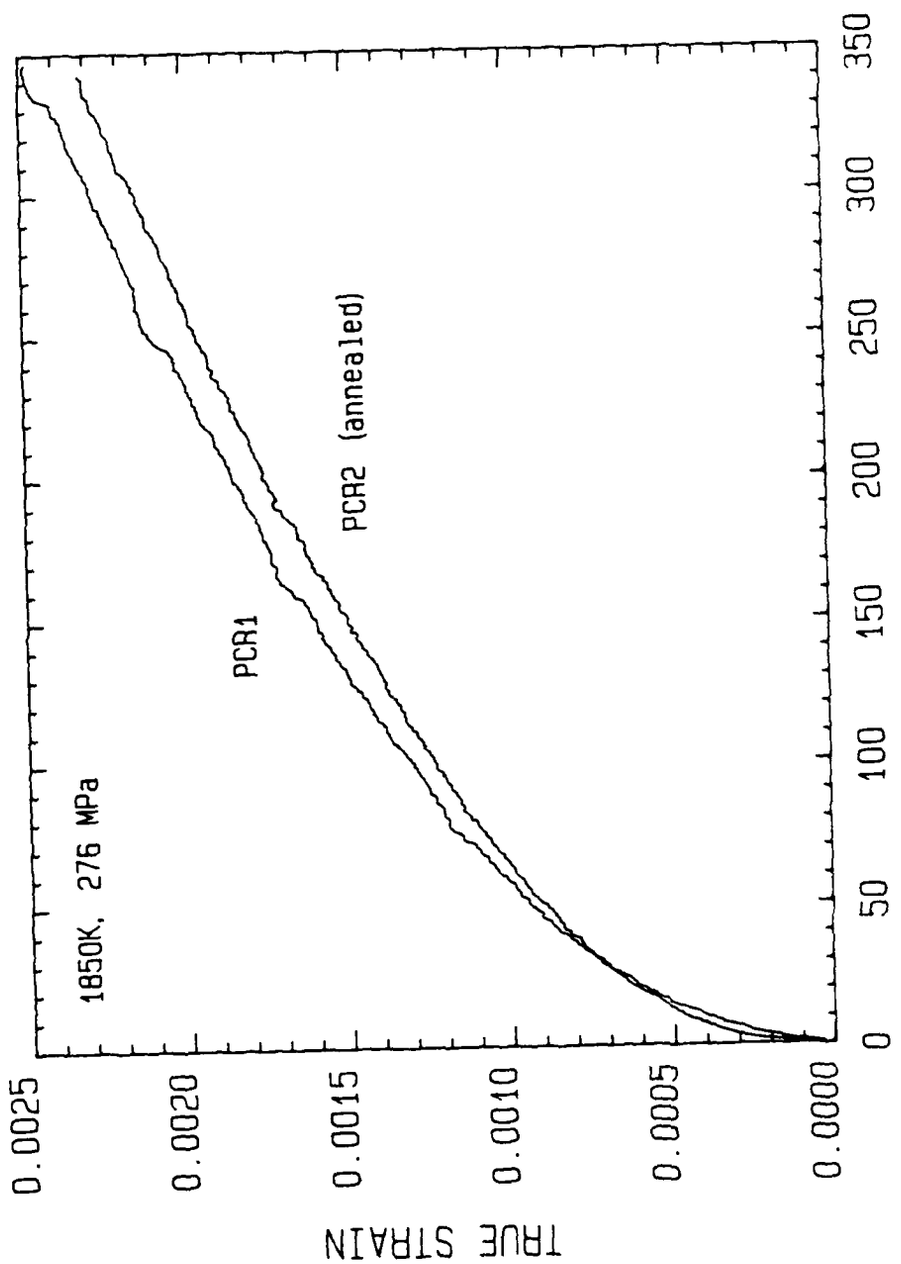

Figure 9: Creep curves from PCR#1 (unannealed) and PCR#2 (annealed) conducted at same stress and temperature.

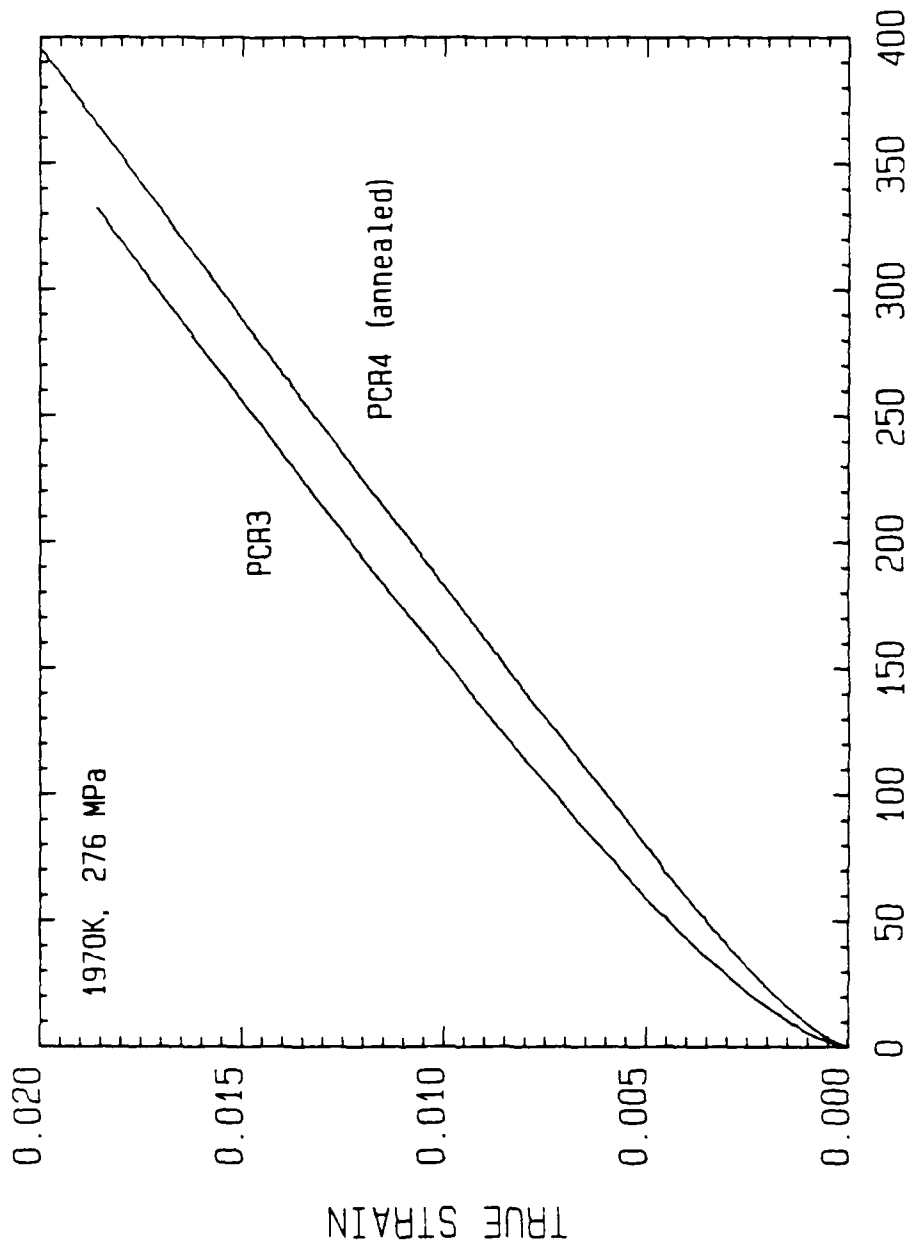

Figure 10: Creep curves from PCR#3 (unannealed) and PCR#4 (annealed) conducted at the same stress and temperature.

all runs to eliminate stress-dependent effects.) Specifically, at 1850K, the initial creep rates of the two samples are essentially the same. However, after ≅40ks (≅11 hours) the rate of deformation of the annealed material begins to slow. This decrease in the creep rate continues to occur very slowly throughout the remainder of the time at temperature; however, both samples appear to be approaching the same steady-state creep rate. By contrast, the creep rates of both materials deformed at 1970K are much faster than their counterparts at 1850K. Furthermore, after only one hour, the creep rate of the annealed material is notably slower than the annealed. However, after ≅150ks (≅41 hours), the creep rates of both materials have again become almost exactly the same.

Additional creep experiments concerned primarily with the initial stage of creep were conducted at 1850K, 276MPa for 10.8ks, 54ks and 162ks and at 1970K, 276MPa for 0.36ks, 36ks and 169.2ks for the purpose of comparative examination of the microstructures at the beginning, the middle and the end of primary creep. It is obvious that the data presented above cannot supply the answers as to the nature of the mechanism(s) responsible for the various stages of creep in the sintered α-SiC material. As such additional evidence must be obtained from visual examination of the as-received, annealed and crept samples via the use of TEM.

C. RESULTS AND DISCUSSION OF TRANSMISSION ELECTRON MICROSCOPY OF SINTERED α-SiC MICROSTRUCTURES

Figures 11, 12 and 13 show the typical microstructures of the as-received annealed (2273K, 24 hours) and crept (find condition was 2020K, 414MPa)samples, respectively. The grains of the first two materials are, for the most part, free of line defects; however, occassional stacking faults do

Figure 11: TEM micrograph of the as-received microstructure.

Figure 12: TEM micrograph of the annealed microstructure. Annealing conditions: 2273K for 24 hours.

Figure 13: TEM micrograph of the crept microstructure. Final creep condition: 2020K, 414 MPa. The total strain was 6%.

occur in selected grains (see upper left of Figure 12) and a few grains contain a substantial number of faults. All of these faults occurred during the fabrication of the SiC powder and not as a result of grinding or piece fabrication. Random dislocations on and off the (0001) plane were also observed. By contrast, a majority of the grains of the crept material were highly faulted as a result of the movement of Shockley partial dislocations through the grain in response to the shear stress on the grain. Finally, although not obvious from these micrographs, the three materials contain B_4C grains, a free C phase and porosity at triple points. The crept material also contains the B-containing precipitates inside the grains as noted earlier and as revealed in Figure 14. These precipitates have not been observed to occur on the grain boundaries.

Another view of the crept material is shown in Figure 15 taken by tilting almost edge-on to the basal plane. This is a most revealing micrograph in that it shows both dislocations (the corrugated lines) as well as stacking faults (the long straight lines). The pinned dislocations are evidence for precipitation. Furthermore, these pinned defects also form into loops which are observed nearly the analogous "hairpin"-shaped dislocations. Figure 16 is a dark held image of the same sample as noted in Figure 15 but taken perpendicular to the basal plane. This view reveals the presence of the B-containing precipitates and dislocation interaction in this (0001) slip plane. Figure 17 is taken from another sample also crept under the final conditions of 2020K, 414MPa and a total strain of 6.0%. This figure was taken somewhat more edge on than Figure 16 and thus better illustrates the presence of dislocation slip bands. Some pinning of dislocations is also observed in this figure.

Figure 14: TEM micrograph of precipitates and stacking faults in a sample crept under the final conditions of 1820K and 414 MPa.

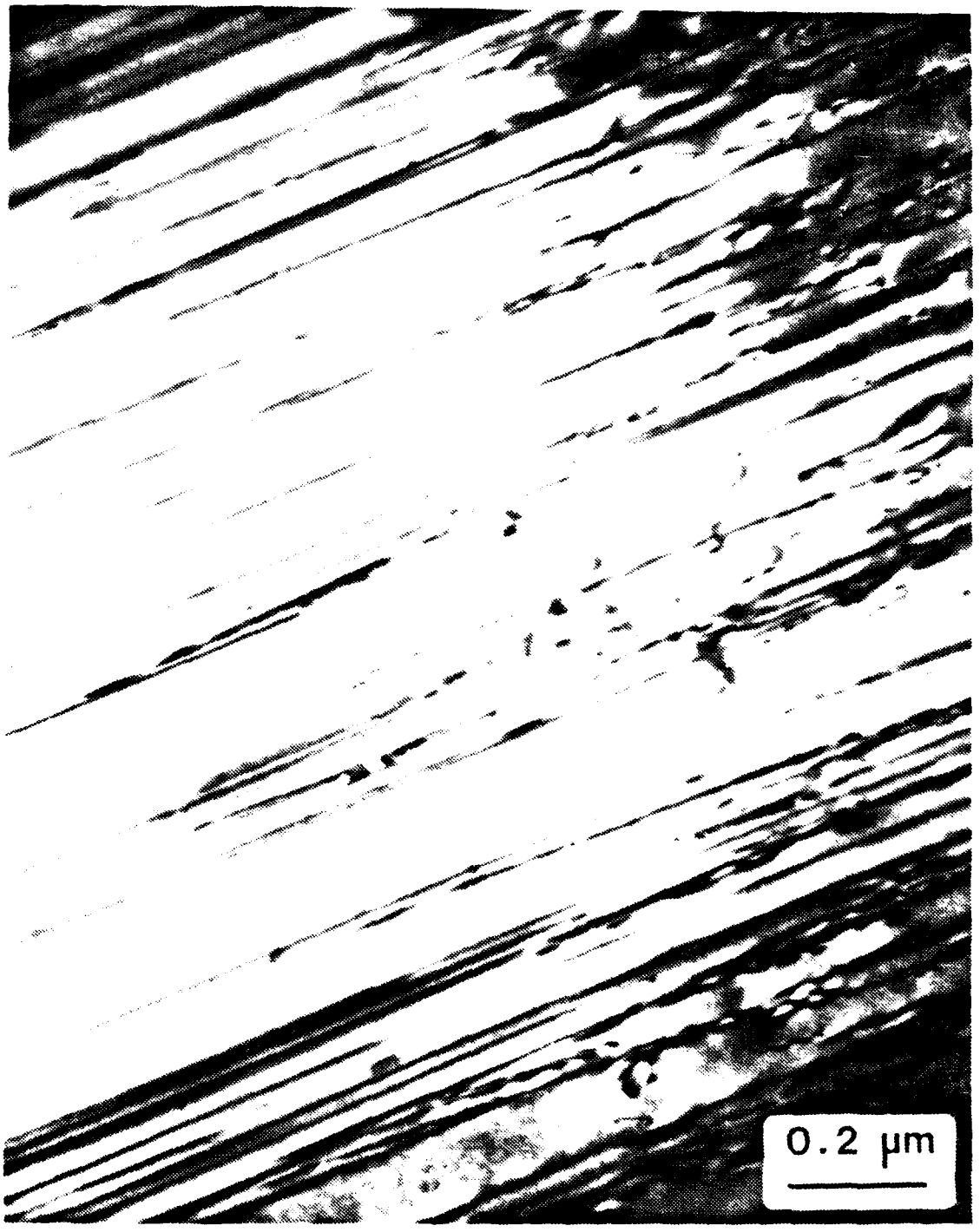

Figure 15: TEM micrograph showing both dislocations (the corrugated lines) and same stacking faults (the long straight lines) in a grain of the crept SiC. Note that some faults end in the grain as a result of the pinning of the leading partial dislocation. Some precipitates and loops are also evident. Final creep conditions 2020K at 414 MPa. The total strain was 8.2%.

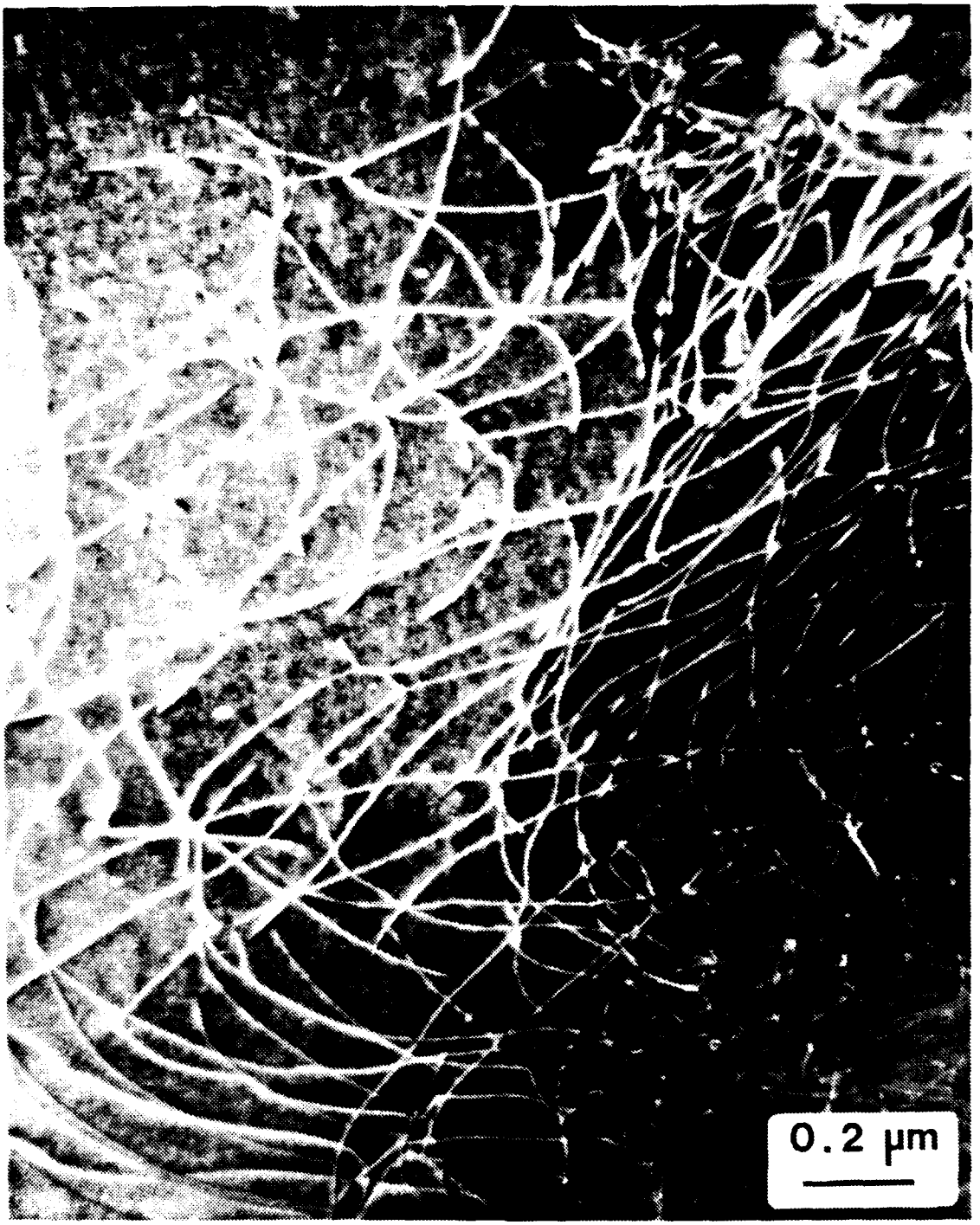

Figure 16: TEM micrograph taken in dark field highlights dislocations and precipitates. Both occur in the (0001) plane. Final creep condition: 2020K at 414 MPa. The total strain was 8.2%.

Figure 17: TEM micrograph showing the high dislocation density typical of the creep samples. Some precipitates are also visible. Final creep conditions: 2020K at 414 MPa; the total strain was 6.0%.

Figure 18: TEM micrograph showing precipitates pinning the leading Shockley dislocations on deformation stacking faults in α-SiC crept at 1820K, 414 MPa to a total strain of 4.7%.

A feature of the stacking faults in the as-received and annealed material is that the stacking faults almost always pass completely through a grain, as seen in Figure 13. By contrast, Figure 18 is a vivid demonstration of the fact that the B-containing precipitates interact with the partial dislocations moving through the material under the influence of the shear stress. Although a portion of the dislocations reach the grain boundaries without interaction with the precipitates, as shown by the right most three dislocations in Figure 18, a major portion are also stopped by the precipitates. To date, we have no evidence of dislocations surmounting these precipitates, even at high temperatures. Additional evidence for the pinning of dislocations is presented in Figure 19 which shows the bowed segments of one large dislocation. Tilting of the sample causes contrast changes which strongly indicate the presence of precipitates at the "pinning" points. Finally, the precipitates occur on the (0001) plane along with the stacking faults and their associated dislocations.

Burgers' vector analyses of the partial dislocations are now ongoing. To assist in this endeavor, a Kikuchi map has recently been developed via the use of TEM samples derived from a high purity single crystal grown via Lely sublimation techniques. To date no evidence of triple point folds, cavitation or dislocation climb has been observed.

D. INTEGRATED ANALYSIS OF RESULTS AND CONCLUSIONS

As noted above, the results of the diffusion data indicate a change in the controlling mechanism of creep at ≅1920K. Furthermore, the values of the stress exponents and the activation energies indicate that creep is controlled above and below this approximate temperature by lattice diffusion and grain boundary diffusion, respectively. Yet, the TEM studies show that an abundance

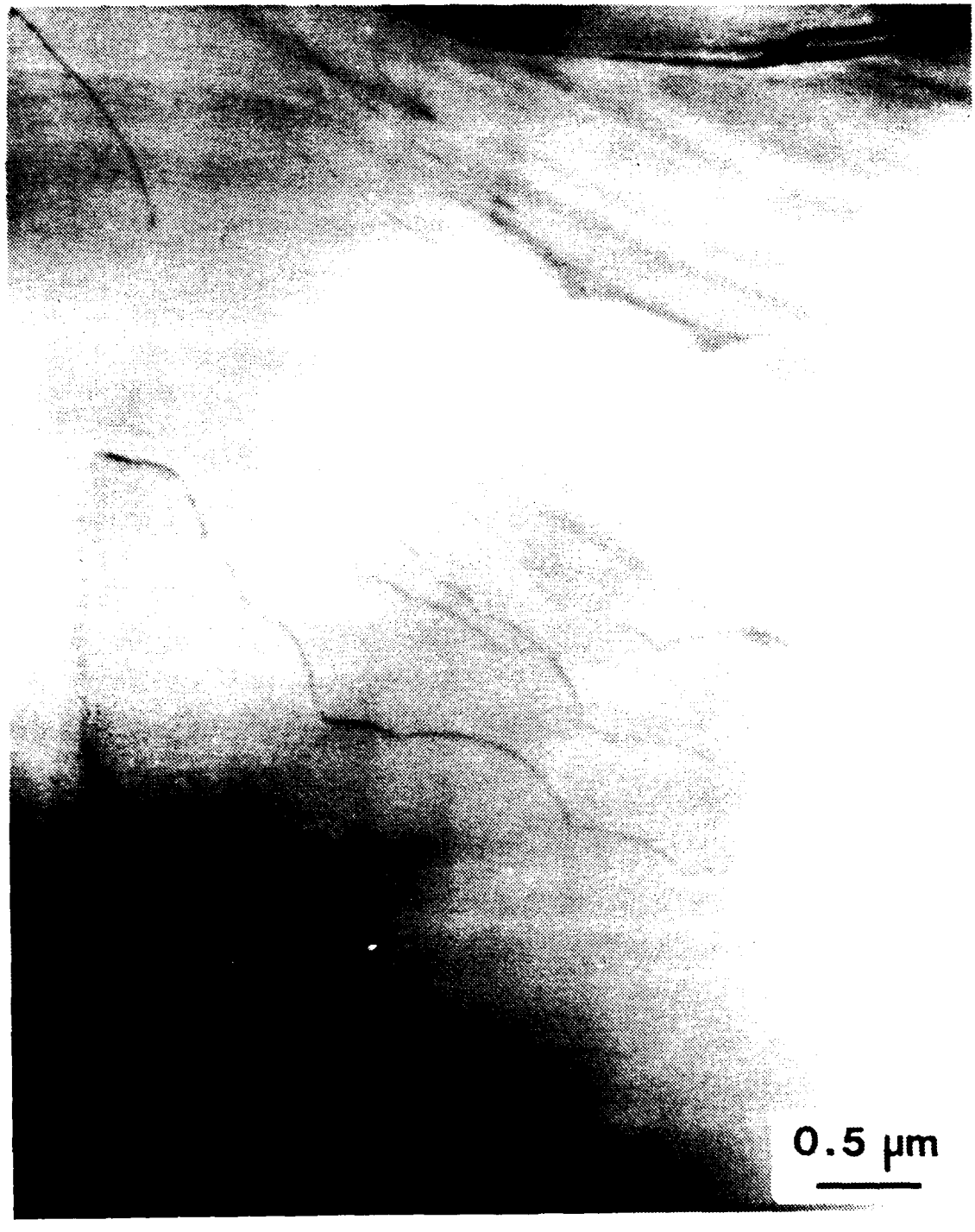

Figure 19: TEM micrograph showing bowed dislocations segments which would indicate precipitates pinning the dislocation. Final creep conditions were 1820K and 414 MPa with a total strain of 4.7%.

of dislocations are generated to allow deformation to occur. Yet these defects are frequently stopped by the appearance and/or the presence of the B-containing precipitates. Although the TEM of the material annealed for short times at the temperatures of creep has not been conducted, it can be expected that the precipitates will nucleate and grow rather quickly once the temperature of deformation has been reached.

Therefore, it may be surmised that the large amount of primary creep in the initial segment of creep is accomodated and, perhaps controlled, by dislocation glide across the grains. However, precipitation is believed to occur during this initial stage which promotes interaction with the moving dislocations to a degree sufficient to cause the steady-state creep to be controlled by mass transport rather than dislocation processes. Thus, diffusion accomodated grain boundary sliding becomes the controlling creep process at high temperatures. Nevertheless, dislocation glide continues to be an active mechanism of deformation but not the controlling process. It should be noted that these results may also signify that since these mechanisms are parallel rather than sequential processes with creep thus being controlled by the fastest mechanism. This implies that self-diffusion in the B-doped materials containing the precipitates is more rapid than dislocation glide. This was not the case for the reaction-bonded and chemically vapor deposited silicon carbides studied previously.

The increasing values of n with increasing temperatures may also indicate that dislocation glide is becoming more important at the higher temperatures. This is reasonable since the solubility of B in SiC increases as the temperature is increased and the amount of supercooling from the temperature of exact total saturation is smaller which should decrease the number of

precipitates which form. This would, in turn, decrease the precipitate-dislocation interaction and enhance the glide process. The high thermal energy input may also assist dislocations in overcoming some of the smaller precipitates. To prove or deny the aforestated hypotheses, further TEM studies are currently ongoing on the crept samples and on the samples crept but stopped at different times into the initial primary stage.

III. NIOBIUM CARBIDE RESEARCH

A. Summary of the Creep Experiments

Constant compressive stress creep experiments have been conducted in the temperature and stress ranges of 1730K - 2100K and 16MN/m^2 - 70 MN/m^2, respectively, on 99.7% dense $NbC_{0.74}$, fabricated by hot isostatically pressing (HIPing) at 2063K under a stress of 206.85 MN/m^2. Stress exponents of 2.0 were determined for stress levels of 16 MN/m^2 - 54 MN/m^2 at all temperatures investigated and 3.2 under stress levels of 54 MN/m^2 - 70 MN/m^2 below 1830K. The activation energy of steady state creep is approximately 230 kJ/mole.

Tables A.1 - A.3 summarize each creep experiment in terms of the conditions of temperature and stress, the times and amounts of primary and total strain, the total amount of creep, the steady-state creep rates observed for each condition of deformation and the stress exponent, n, and activation energy, Q, determined from several sets of conditions. These tables will be referenced following the discussion regarding the results of the transmission electron microscopy (TEM) studies.

Table A.1: Conditions of Temperature and Constant Stress Employed for Creep Experiments in this Research.

Run#	Condition	Density (% Theoretical)	Temperature (K)	Stress (MN/m^2)
1	1	99.7	1973	16.40
	2		2010	16.40
	3		2050	16.40
	4		2100	16.40
	5		2100	19.90
	6		2100	23.40
	7		2100	30.25
2	1	99.7	1770	36.76
	2		1770	40.09
	3		1770	43.96
	4		1770	47.47
	5		1770	53.94
	6		1830	53.94
	7		1880	53.94
	8		1930	53.94
3	1	99.7	1730	34.60
	2		1730	41.03
	3		1730	48.00
	4		1830	48.00
	5		1930	48.00
	6		1830	48.00
	7		1830	55.31
	8		1830	62.45
	9		1830	69.20
4	1	97.0	1900	47.10
	2		2000	47.10
	3		2100	47.10
5	1	97.0	1730	34.54
	2		1730	41.46
	3		1730	48.95
6	1	97.0	1900	16.60
	2		2000	16.60
	3		2100	16.60

Table A.2: Time Elapsed in Primary Strain, Amount of Primary Strain, Total Time Elapsed for a Given Condition, Total True Strain and Total Amount of Creep for each Creep Condition.

R,C*	Time in Primary (ks)	Primary Strain	Total time (ks)	Total True Strain	Total Creep (um)
1,1	170	0.0056	328	0.0081	63
1,2	92	0.0024	507	0.0171	90
1,3	95	0.0017	938	0.0202	156
1,4	126	0.0033	1180	0.0258	198
1,5	100	0.0026	1369	0.0316	242
1,6	115	0.0054	1626	0.0430	328
1,7	115	0.0183	1935	0.0734	551
2,1		0.0048	190	0.0061	46
2,2	130	0.0021	422	0.0099	73
2,3	141	0.0029	663	0.0144	107
2,4	119	0.0024	856	0.0182	135
2,5	134	0.0038	1115	0.0257	191
2,6	135	0.0049	1288	0.0334	246
2,7	116	0.0076	1486	0.0455	334
2,8	122	0.0160	1731	0.0674	489
3,1	153	0.0009	244	0.0015	12
3,2	155	0.0013	491	0.0035	27
3,3	137	0.0018	750	0.0066	50
3,4	120	0.0046	998	0.0157	120
3,5	130	0.0093	1220	0.0308	234
3,6	78	0.0015	1470	0.0360	272
3,7	118	0.0037	1722	0.0441	332
3,8	92	0.0048	1988	0.0574	430
3,9	100(I)+	0.0082	2248	0.0790	586
4,1	240	0.0178	517	0.0236	178
4,2	60(I)	0.0049	753	0.0436	325
4,3	75(I)	0.0234	926	0.0998	725
5,1	156	0.0015	261	0.0022	17
5,2	134	0.0013	489	0.0044	34
5,3	155	0.0017	749	0.0074	57
6,1	214	0.0041	319	0.0052	41
6,2	113	0.0046	481	0.0114	89
6,3	119	0.0063	655	0.0200	154

*R = Run #; C = Condition as noted in the first two columns in Table A.1.

+The letter "I" indicates an inverted primary region.

Table A.3: Values of Steady-State Creep Rate for each Condition, Stress Exponent, n, and/or Activation Energy, Q, for each Creep Experiment.

R,C*	Steady State Creep Rate(s^{-1})	Log $\dot{\varepsilon}$	Log σ	ln $\dot{\varepsilon}$	$10^4/T$	n and/or Q
1,1	1.55×10^{-8}			-17.98	5.07	
1,2	1.76×10^{-8}			-17.86	4.98	Q=72.5
1,3	1.87×10^{-8}			-17.80	4.88	kJ/mol
1,4	1.98×10^{-8}	-7.69	1.21	-17.71	4.76	
1,5	3.00×10^{-8}	-7.52	1.30			
1,6	4.34×10^{-8}	-7.36	1.37			n=2.02(3)†
1,7	9.58×10^{-8}	-7.02	1.48			n=2.57(4)
2,1	9.20×10^{-9}	-8.04	1.57			
2,2	1.59×10^{-8}					n=2.05(4)
2,3	1.59×10^{-8}	-7.80	1.64			
2,4	1.83×10^{-8}	-7.74	1.68			
2,5	2.28×10^{-8}	-7.64	1.73	-17.60	5.65	
2,6	3.90×10^{-8}			-17.06	5.46	Q=231
2,7	5.49×10^{-8}			-16.72	5.32	kJ/mol
2,8	8.09×10^{-8}			-16.27	5.18	
3,1	5.39×10^{-9}	-8.27	1.54			
3,2	8.27×10^{-9}	-8.08	1.61			n=2.01
3,3	1.04×10^{-8}	-7.98	1.68	-18.38	5.78	
3,4	3.36×10^{-8}			-17.21	5.47	Q=249
3,5	6.25×10^{-8}			-16.59	5.18	kJ/mol
3,6	2.08×10^{-8}	-7.68	1.68			
3,7	3.20×10^{-8}	-7.49	1.74			n=3.2(3)
3,8	4.85×10^{-8}	-7.32	1.80			
3,9	8.56×10^{-8}	-7.07	1.84			
4,1	1.97×10^{-8}			-17.74	5.26	Q=458(2)
4,2	8.46×10^{-8}			-16.29	5.00	kJ/mol
4,3	3.39×10^{-7}			-14.90	4.76	Q=475(3) kJ/mol
5,1	4.29×10^{-9}	-8.37	1.54			
5,2	7.92×10^{-9}	-8.10	1.62			n=2.07
5,3	8.76×10^{-9}	-8.06	1.69			
6,1	1.11×10^{-8}			-18.32	5.26	Q=206 (3)
6,2	3.16×10^{-8}			-17.27	5.00	kJ/mol
6,3	3.80×10^{-8}			-17.09	4.76	

*R = Run #; C = Condition as noted in the first two columns in Table A.1.

†The numbers in parenthesis are the number of data points used to make the stress exponent or activation energy calculation. In each case, the smaller number refers to the first points obtained during the given run.

B. Summary of Studies By Transmission Electron Microscopy

Microstructural studies by TEM at Oak Ridge National Laboratory and North Carolina State University have been performed on all samples. Results of this study on the as-HIPed but unannealed material reveal grown-in low angle dislocation tilt and twist subboundaries (Figure 1-A) and dislocation tangles (Figure 1-B) generated during the HIPing process. The structures of Figure 1-A are also typical of the crept material, a characteristic which should be expected since hot-isostatic pressing involves deformation of a powder compact.

Prior to the creep experiments, the HIPed $NbC_{0.74}$ was annealed at 2173K for 272 ks to remove oxygen and stabilize the grain size. The grain size increased dramatically, and some of the dislocation structures present in the HIPed material were incorporated in the moving boundaries. Figures 2-A and B represent the typical dislocation structures present in the annealed material, the starting material for creep research. Figure 2-A is a subgrain boundary (common in this material) consisting of a set of straight dislocations labeled (a) in the micrograph and another set of dislocations labeled (b), (c) and (d) which form a similar type of boundary in another plane. A Burgers vector analysis shows the dislocations at (a) to be of mixed character and lying on the (111) plane with Burgers vector b=a/2[011]. The other boundary of dislocations which are in the (111) plane are part of another mixed boundary which appears to be knitted. Figure 2-B shows a twist boundary which is similar to the one in Figure 1-A.

The dislocation structure of the annealed material is not homogeneous; that is, the subboundaries are not uniformly distributed throughout each grain. In addition, several grains do not have many dislocations, as shown in

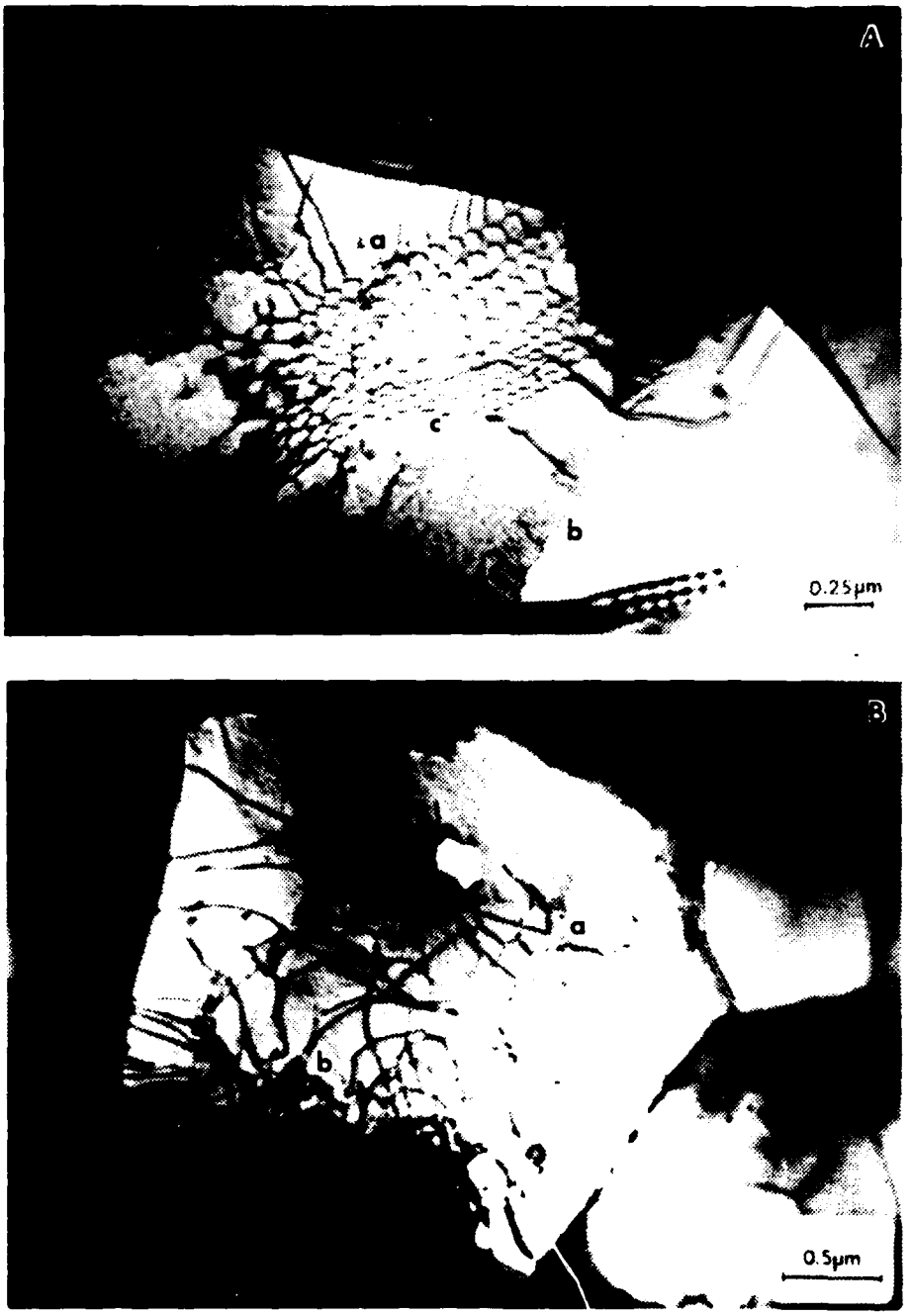

Figure 1. TEM micrographs of 99.7% dense $NbC_{0.74}$ HIPed for 7.2 ks at 2063K under a stress of 206.85 MN/m^2. A) Twist (regions a and c) and tilt (region b) subboundaries. B) Typical grain with poorly defined subboundary (region a) and tangled dislocations (region b).

Figure 2. TEM micrographs of annealed 99.7% dense $NbC_{0.74}$. A) Mixed dislocation subboundary. The Burgers' vectors of the labeled dislocations are as follows: a: b = a/2[011], b: b = a[101], c: b = a/2[011], d: b = a/2[1$\bar{1}$0]. B) Twist boundary. Note the dislocation dissociation in regions a and b in this figure.

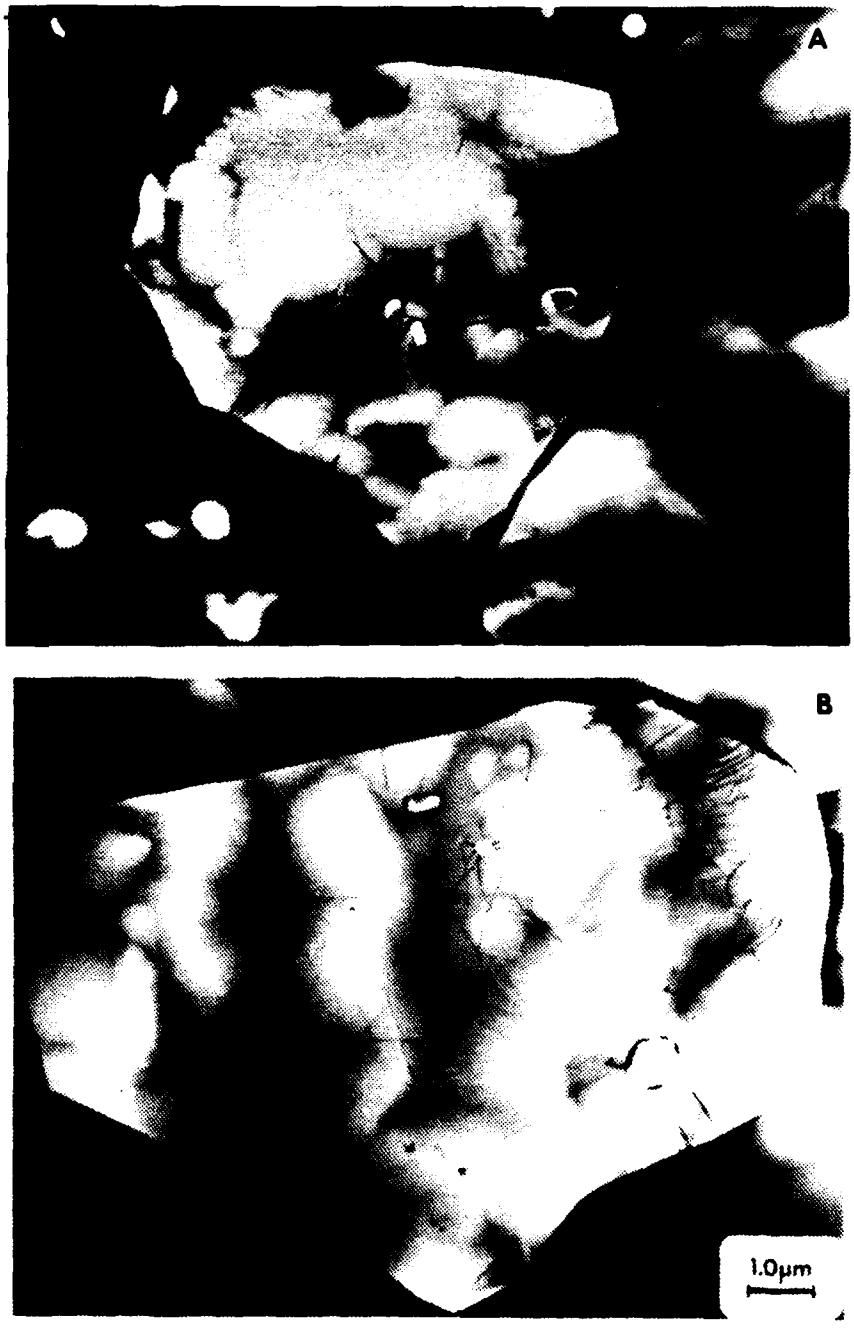

Figure 3. TEM micrographs of annealed 99.7% dense $NbC_{0.74}$
A) Grain with low dislocation density.
B) Heterogeneous dislocation structure. Notice that the subboundary exists in only one region of the grain.

Figure 3-A. Other grains have subboundaries which exist in a small portion of the grain as shown in Figure 3-B. This latter structure will explain how primary creep occurs in this material, as discussed in section (C).

Microscopy of the crept materials also reveals that the movement and generation of dislocations are involved during the deformation of $Nb_{0.74}$ at 1730K (the lowest temperature employed in this research and just above the brittle-ductile transition temperature) and under stresses of 34 MN/m^2-54 MN/m^2, the subboundaries in the annealed material are broken into loose dislocations as shown in the composite micrograph in Figure 4. Notice the presence of dislocation dipoles at this temperature. There is not TEM evidence for well defined long subboundaries at 1730K, as observed in the annealed material.

At 1830K and under stresses of 54 MN/m^2 - 70 MN/m^2, the subboundaries are well defined tilt boundaries of mixed dislocations which are different than the hexagonal networks in the annealed sample. In addition, these boundaries are knitted, as shown in Figure 5, which indicates more glide activity than was observed at lower stress. A Burgers vector analysis of the dislocations in this figure indicate that the subboundary consists of dislocations (a) which lie on the (111) plane with Burgers vector $a/2[110]$. The (b) dislocations lying on the (111) plane appear to knit into the (a) dislocations forming a junction dislocation on the (111) plane with Burgers vector $a[101]$. Knitting occurs by dislocations gliding to the subboundary and then knitting the boundary by stress-induced climb or glide. It appears that dislocation (c) simply glides into the boundary without knitting.

At 1930K and under stresses of 34-54 MN/m^2, more complicated dislocation networks form. Most of the subboundaries are hexagonal and are curved,

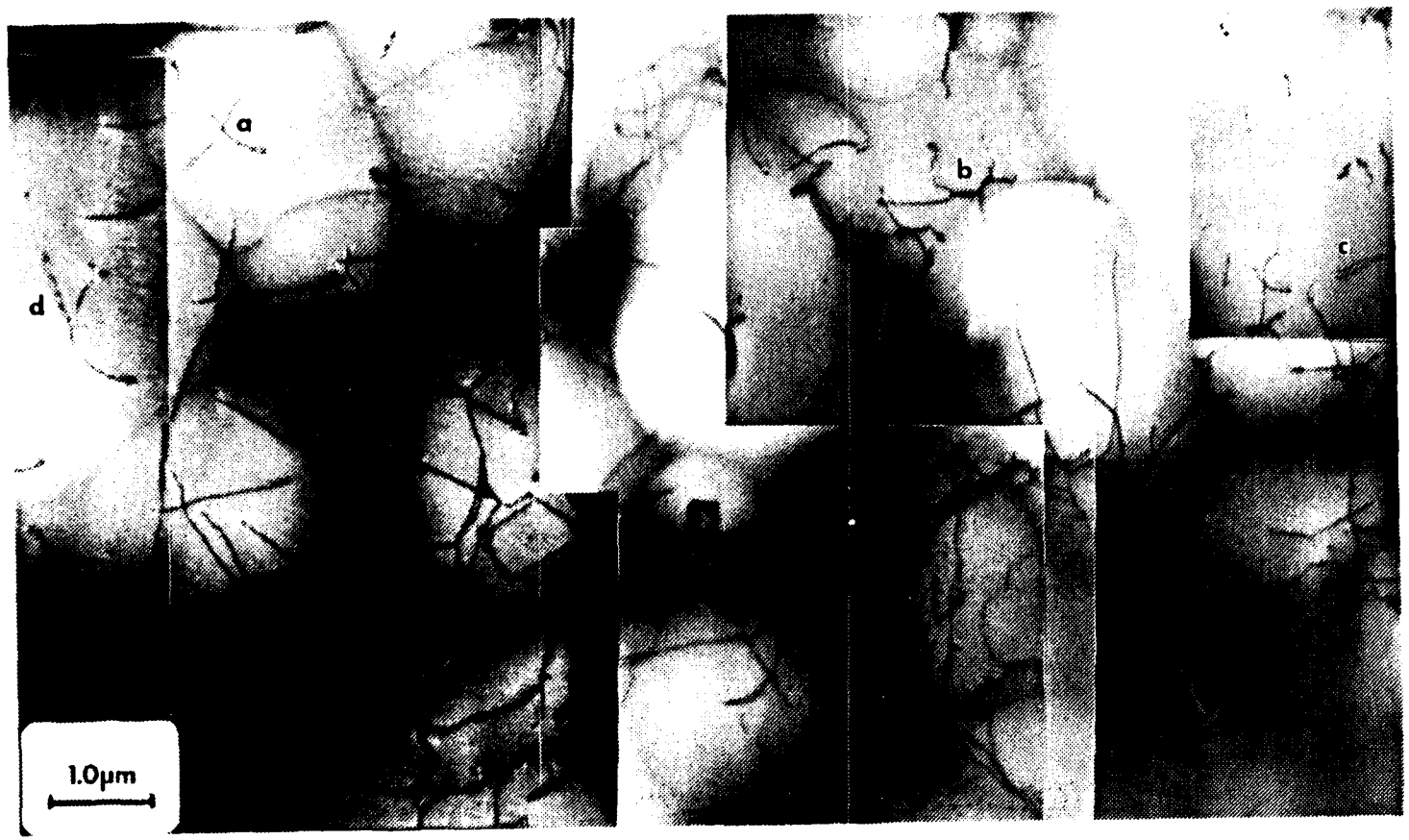

Figure 4. TEM micrograph of $NbC_{0.74}$ crept at the final conditions of 1730K and 48.95 MN/m^2. The well-defined dislocation sub-boundaries established during the anneal have been broken into loose dislocation. Notice the presence of dislocation dipoles (for example, in region a and b).

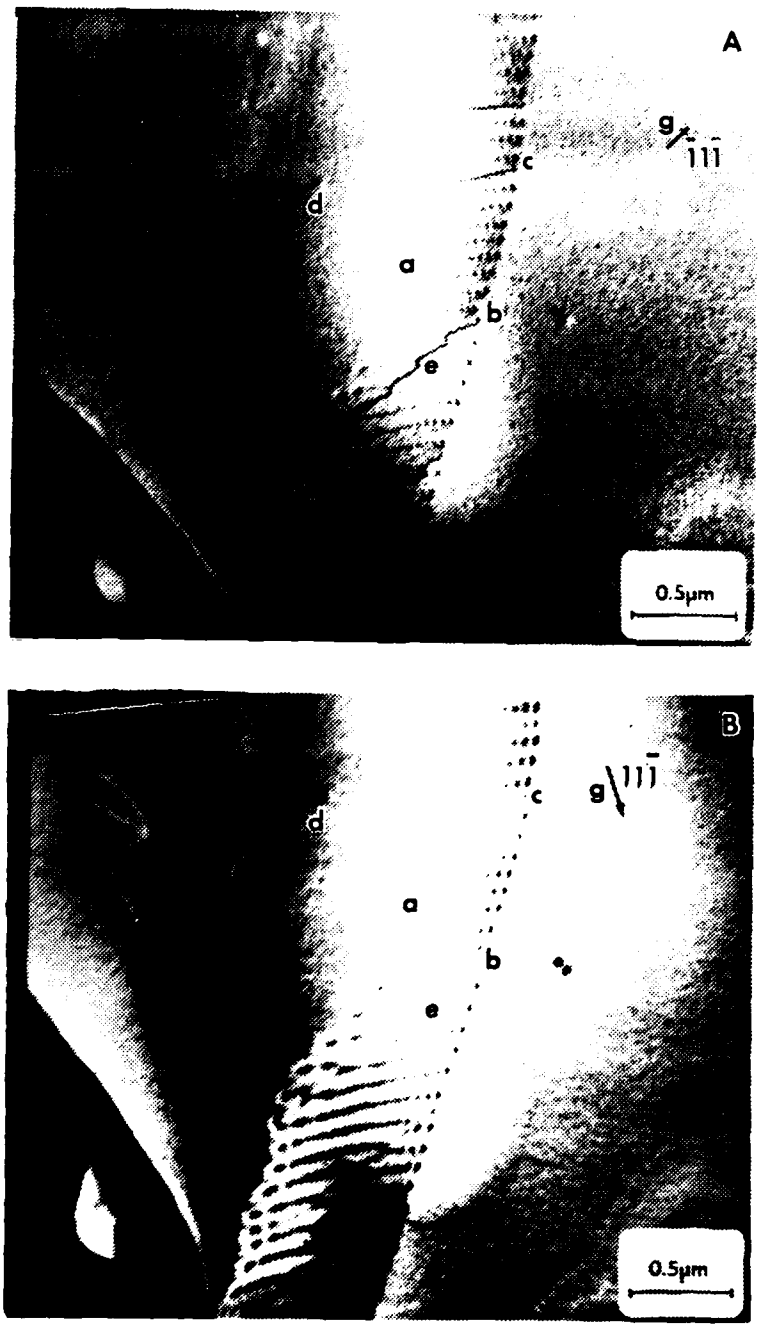

Figure 5. TEM micrograph of $NbC_{0.74}$ crept at the final conditions of 1830K and 69.20 MN/m^2. A) and B) show a knitted mixed dislocation subboundary. The Burgers' vectors of the labeled dislocation are as follows: a,d: b = a/2[011], b,c: b = a/2[1$\bar{1}$0], e: b = a[101].

Figure 6. TEM micrograph of $NbC_{0.74}$ crept at the final conditions of 1930K and 54 MN/m^2. Curved hexagonal dislocation subboundary. Notice the large number of free dislocations inside the subgrain.

indicating subboundary movement, as shown in Figure 6. Even though this micrograph was taken using a one million volt electron microscope, it is evident that more slip systems are involved in the creep process at 1930K, since more dislocation interaction occurs.

At higher temperatures near 2100K and under stresses of 16 MN/m^2 - 30 MN/m^2, the subboundaries are quite similar to the ones established at 1930K, though they are even more well-defined (polygonized), as shown in Figure 7-A and B, indicating more climb activity (and thus recovery inside the grain). All of the subboundaries are curved.

Figure 8 compares the knitted subboundaries at 1830K and 2100K, respectively. As shown in Table A.1, the final stress at 1830K in the third experiment is approximately 70 MN/m^2. The final stress at 2100K in the first experiment is approximately 30 MN/m^2. The micrographs in this figure indicate that more knitting and subboundary movement occurs at higher temperature. Thus knitting at lower temperature appears to occur by glide and at higher temperature by glide and climb. This result indicates that more recovery (dislocation annihilation) can occur at higher temperature.

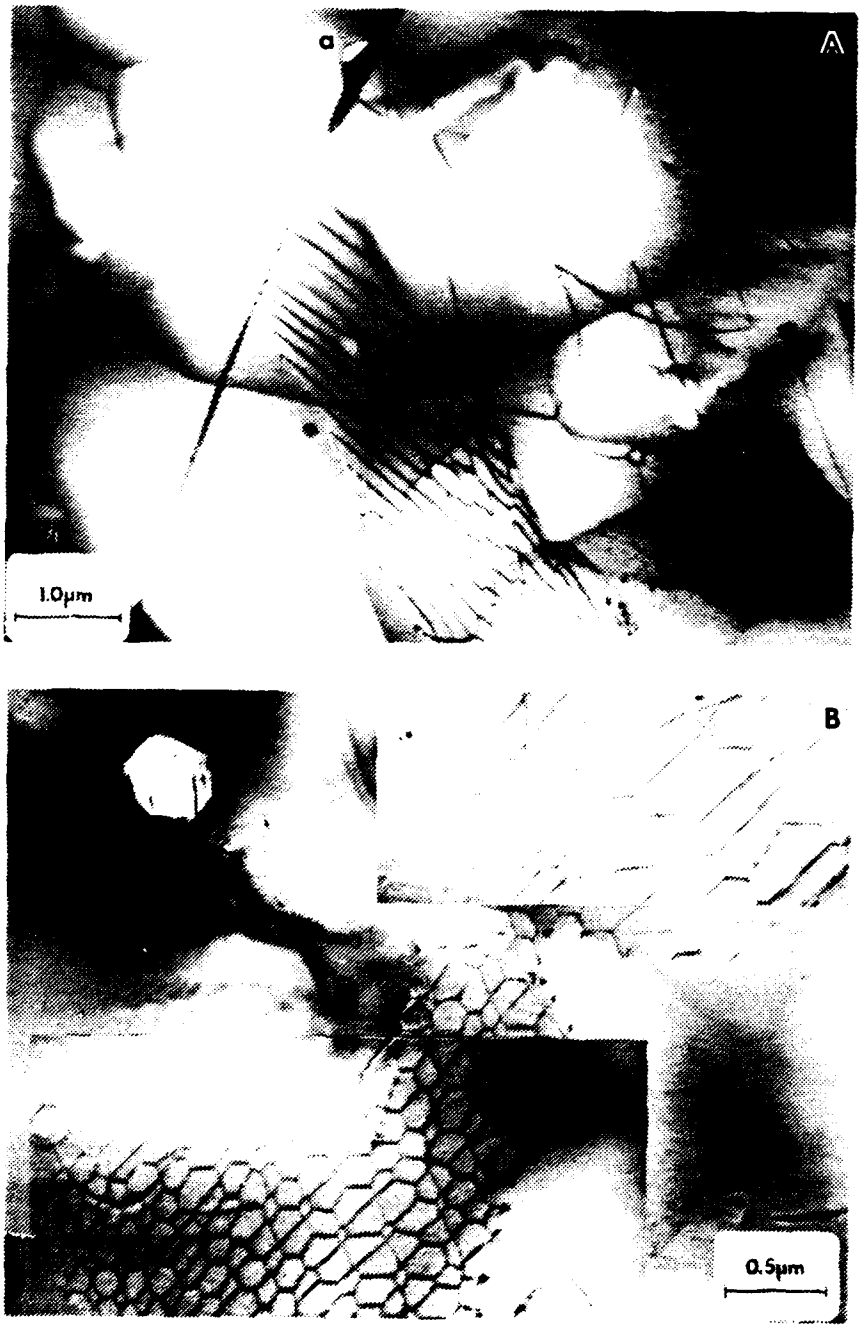

Figure 7. TEM micrographs of $NbC_{0.74}$ crept at the final conditions of 2100K and 30.25 MN/m^2. A) and B) are well-defined hexagonal networks formed by the interaction of three sets of dislocations.

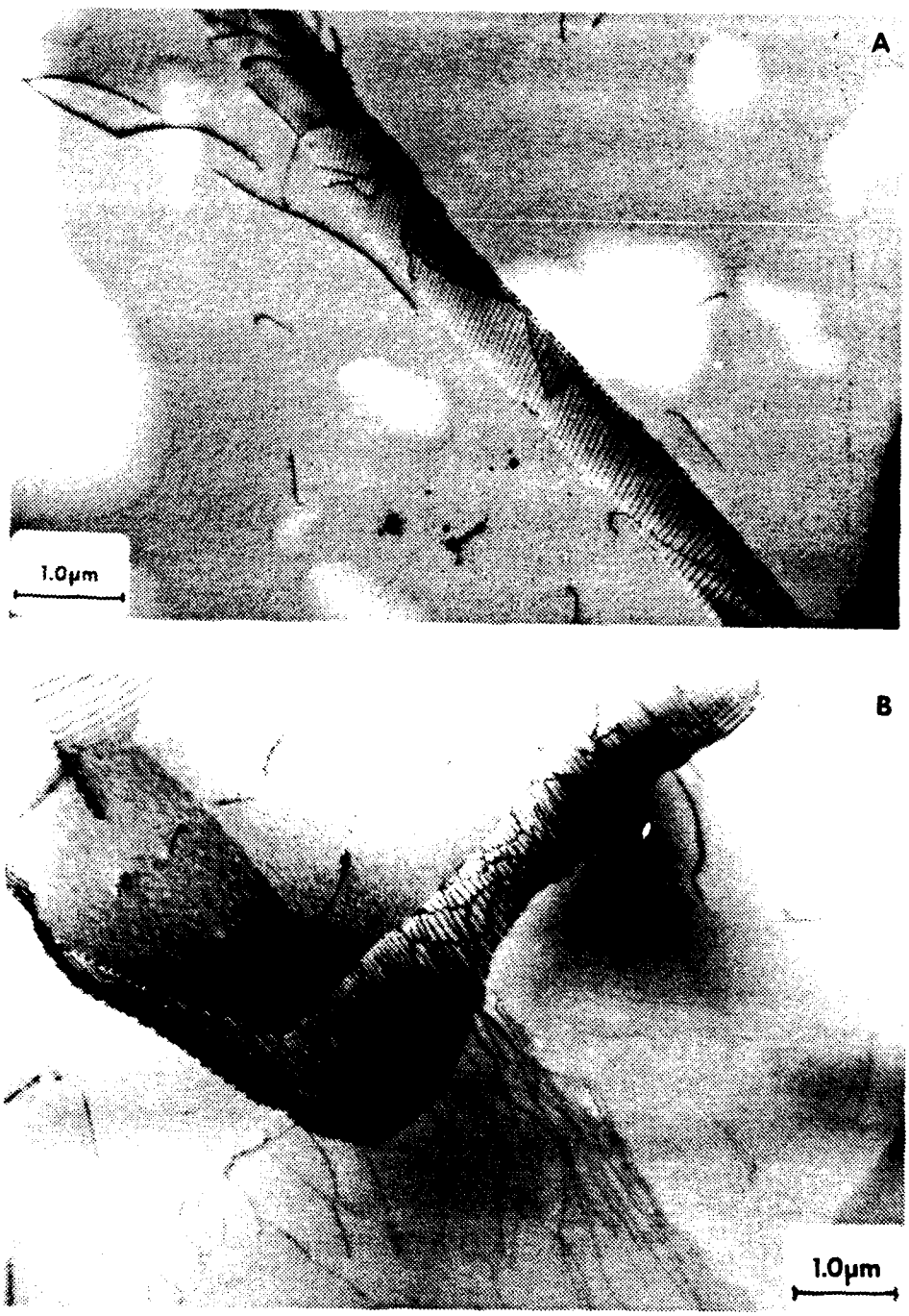

Figure 8. TEM micrographs of crept $NbC_{0.74}$ comparing the knitted sub-boundaries formed under creep at low and high temperature. A) 1830K, 69.20 MN/m^2. B) 2100K, 47 MN/m^2. More knitting occurs at the higher temperature due to an increase in the amount of dislocation climb.

C. Discussion of Creep Mechanisms in $NbC_{0.74}$

1. Primary Creep

The creep curve for each condition of each creep experiment showed two regions of deformation; primary (transient) and secondary (steady-state). Though this research is primarily concerned with the results of the secondary region (n, Q, and TEM structure), it is important to mention a few characteristics of primary creep and the primary creep strain observed at each condition.

Table A.2 indicates that the annealed sample, upon loading, undergoes a certain amount of primary strain prior to steady-state creep. At the initial condition, the amount of primary strain is greater than that experienced at the second condition, probably as a result of the easy glide and the long glide paths of the dislocations allowed by the inhomogeneous dislocation structure present in the annealed material. The creep rate subsequently slows as the gliding dislocations encounter the grown-in dislocation forests until steady-state creep occurs. An increase in stress or temperature (new condition) following the initial period of steady-state creep results in additional primary strain. However, since the concentration of dislocations is now much higher than at the beginning of the experiment, strain hardening and recovery occurs much more rapidly which causes the second region of primary creep to be less (see run #2, condition 2). Nevertheless, with increasing stress and/or temperature following the second condition the amount of primary strain at subsequent conditions is greater relative to that found in the previous portion of primary creep of the same run (see for example, run #2, conditions 5-8). This marked increase in primary creep is believed to be caused by an enhancement of the factors which are responsible for the renewal

of primary creep in the first place; the enhanced ability of the pinned dislocations to break away from their intersections with other dislocations and other physical barriers, the increased activity of dislocation sources and the higher velocity of glide which the dislocations experience as a result of the increased stress and/or temperature.

2. Steady-State Creep

Steady-state creep occurs as a result of the balance between strain hardening and recovery. An n value of 2.0 and activation energy of 230 kJ/mole as well as the lack of evidence for subboundary formation indicate that at low temperature (1730K (just above the brittle-ductile transition temperature of polycrystalline $NbC_{0.74}$)) and low stress where dislocation glide activity is limited, that grain boundary sliding contributes to creep. The activtion energies of creep are significantly lower than those for lattice self-diffusion (see Table C.1). The activation energy for grain boundary diffusion is normally 0.6 - 0.7 Q , which would be for carbon diffusing along the grain boundary, approximately 190.6 - 222.6 kJ/mole. At 1830K and under higher stresses which gave a stress exponent of 3.2 (indicative of a lattice mechanism of creep), dislocation glide accounts for the strain, and recovery occurs by dislocations being absorbed on the grain boundary. At higher temperatures (above 1930K) strain occurs by dislocation glide and subboundary movement and recovery by dislocation annihilation within the subboundary. It is suspected that the lower n and Q values of 2.0 and 206 kJ/mole, respectively, at higher temperature results from the increase in impurity assisted creep.

Table C.1: Activation energy values for self-diffusion of the metal and nonmetal species in single crystalline NbC_x [1,2].

Composition	Species	Activation Energy, kJ/mol
0.766	C	317.7±11.3
0.834	C	419.7±9.24
0.868	C	438.9±13.8
All	Nb	585.2±10.0

---

[1]Yu and Davis, J. Phys. Chem. Solids, 40, 997 (1979).

[2]Yu and Davis, J. Phys. Chem. Solids, 51, 261 (1979).

IV. PUBLICATIONS AND TECHNICAL REPORTS FROM THIS RESEARCH

A. Publications

1. C. H. Carter, Jr., R. F. Davis and J. Bentley "Kinetics and Mechanisms of High-Temperature Creep in Silicon Carbide: I. Reaction-Bonded," J. Am. Ceram. Soc. 67, 409 (1984).

2. C. H. Carter, Jr., R. F. Davis and J. Bentley, "Kinetics and Mechanisms of High-Temperature Creep in Silicon Carbide: II. Chemically Vapor Deposited. Ibid., 732 (1984).

3. C. H. Carter, Jr., J. Bentley and R. F. Davis, "The Occurence of Defects in Silicon Carbides as a Result of Processing Mode and Applied Stress," presented at and published in "Defect Properties and Processing of High Technology Non-metallic Materials, Materials Research Society Symposia Proceedings Vol. 24, J. H. Crawford, Jr., Y-Chen, and W. A. Sibley, Eds., North Holland, New York, pp. 351-364, 1984.

4. R. F. Davis, "Hot Isostatic Pressing of Ceramic Materials" Encyclopedia of Materials Science and Engineering, Vol. 3, M. B. Bever, Ed-in-Chief, Pergamon Press, New York, N.Y., pp. 456-483 (1985). This article was also published in the Journal of Materials Education 6, 157 (1984).

5. R. F. Davis, J. E. Lane, C. H. Carter, Jr., J. Bentley, W. H. Wadlin, D. P. G. Griffis, R. W. Linton, and K. L. More, "Microanalytical and Microstructural Analyses of Boron and Aluminum Regions in Sintered Alpha Silicon Carbide", Scanning Elec. Micros. 1984, 1161 (1984).

6. R. F. Davis, C. H. Carter, Jr., S. Chevacharoenkul and J. Bentley, "The Occurrence and Behavior of Dislocations During Plastic Deformation of Selected Transition Metal and Silicon Carbides", Deformation of Ceramics II, R. E. Tressler and R. C. Bradt, eds., Plenum, New York, 97 (1984).

7. R. F. Davis, "High Temperature Creep in Reaction-Bonded and Chemically Vapor Deposited Silicon Carbides" invited paper presented at the NSF/JSPS-US/Japan Seminar on Structural Ceramics, University of Washington, Seattle, WA, August 13-15, 1984. To be published.

8. K. L. More, J. Ryu, C. H. Carter, Jr., J. Bentley and R. F. Davis, "Defects in SiC-Their Electrical and Physical Consequences", invited paper presented at the International Conference on Defects in Insulating Crystals, University of Utah, Salt Lake City, UT, August 20-24, 1984. To be published as a book-journal by Gordon and Breach.

9. H. H. Ledbetter, S. Chevacharoenkul and R. F. Davis, Monocrystal Elastic Constants of NbC, submitted to the J. Appl. Physics.

B. Technical Reports

1. Interim Technical Reports submitted to the Army Research Office and to the National Science Foundation

   a. December, 1982
   b. July, 1983
   c. December, 1983
   d. July, 1984
   e. December, 1984

2. Final Report submitted to the Army Research Office and to the National Science Foundation on August, 1985.

V. PARTICIPATING SCIENTIFIC PERSONNEL

A. Principal Investigator - Robert F. Davis

B. Post Doctrates - Calvin H. Carter, Jr.

C. Graduate Research Assistants and Degrees Awarded

1. Calvin H. Carter, Jr. - Ph.D.
2. Sopa Chevacharoenkul - Ph.D.
3. Robert M. Nixon - M.S.
4. Jay E. Lane (Ph.D. in progress)

END

FILMED

1-86

DTIC